Increased functional potency of multi-edited CAR-T cells manufactured by a non-viral transfection system

Aine O'Sullivan,[1] Sarah Case,[1,3] Aisling McCrudden,[1,3] Emer Hackett,[1] Louise Gallagher,[1] Darren Martin,[1] Gillian P. Johnson,[1] Kirti Mahadik,[1] Thomas Kienzle,[1] Jude Kevin Lim,[1] Aya Nashat,[1] Kartik Srinivasan,[1] Mark W. Lowdell,[2] Lisa O'Flynn,[1] and Jamie Frankish[1]

[1]Avectas, Cherrywood Business Park, Dublin, Ireland; [2]University College London, Cancer Institute, London, UK

Chimeric antigen receptor (CAR)-T cell therapy represents a breakthrough for the treatment of hematological malignancies. However, to treat solid tumors and certain hematologic cancers, next-generation CAR-T cells require further genetic modifications to overcome some of the current limitations. Improving manufacturing processes to preserve cell health and function of edited T cells is equally critical. Here, we report that Solupore, a Good Manufacturing Practice-aligned, non-viral physicochemical transfection system, can be used to manufacture multi-edited CAR-T cells using CRISPR-Cas9 ribonucleoproteins while maintaining robust cell functionality. When compared to electroporation, an industry standard, T cells that were triple edited using Solupore had reduced levels of apoptosis and maintained similar proportions of stem cell memory T cells with higher oxidative phosphorylation levels. Following lentiviral transduction with a CD19 CAR, and subsequent cryopreservation, triple-edited CAR-T cells manufactured using Solupore demonstrated improved immunological synapse strength to target CD19^{+} Raji cells and enhanced cellular cytotoxicity compared with electroporated CAR-T cells. In an *in vivo* mouse model (NSG), Solupore triple-edited CAR-T cells enhanced tumor growth inhibition by more than 30-fold compared to electroporated cells.

INTRODUCTION

Chimeric antigen receptor (CAR)-expressing T cell therapies have revolutionized the clinical approach to hematological malignancies and now offer effective treatment options in relapsed and refractory indications.[1–6] At the beginning of 2024, over 1,800 clinical trials have investigated CAR-T therapies, with over 30,000 patients receiving a CAR-T cell treatment since the first US Food and Drug Administration (FDA)-approved product in 2017.[7] Despite some clinical success resulting in six FDA-approved CAR-T therapies, the overall response rate (ORR) in many indications is poor.[8,9] Advancements in addressing the challenges of CAR-T cell use in the clinic are being made.[10] Of late, there has been a shift in focus to addressing the impact of manufacturing processes on the phenotype of CAR-T cell products and their functional capacity for clinical use. The rare T cell subset

population, known as stem cell memory cells (T_{SCM})[11,12] has been shown to confer greater levels of engraftment, expansion, and persistence *in vivo*,[13–17] ultimately resulting in a more potent and durable targeted cytotoxic response. Despite some level of plasticity within T cell subsets that are, at least in part, terminally differentiated to central memory or effector memory T cells *in vitro*,[18] the maintenance or retention of T_{SCM} cells is of critical importance when manufacturing CAR-T cells for clinical therapies.[19] Thus, reducing the length of the *in vitro* expansion phase may yield higher quantities of T_{SCM} cells. In support of this, the rapid manufacturing approach applied in the anti-BCMA CAR-T, durcabtagene autoleucel (T-Charge) (the study was registered at ClinicalTrials.gov: NCT04318327),[20] and the dual-targeting BCMA CD19 CAR-T, GC012F studies, demonstrated a 100% ORR in relapsed/refractory multiple myeloma (r/rMM) (these studies were registered at ClinicalTrials.gov: NCT04236011 and NCT04182581).[21,22] It is apparent that further advancements throughout the CAR-T manufacturing process are required to produce CAR-T cells that are healthier, metabolically fitter, and more effective clinically, without compromising the safety profile of the product.[23] As such, improvements in genetic engineering methods to maximize cell fitness of complex and advanced CAR-T products, through manufacturing processes, are of pivotal importance for improving clinical outcomes. A non-viral standard for delivering gene-modifying cargo to target cells is reversible electroporation, which temporarily increases the membrane permeability to otherwise impermeable cargo using an electric pulse of sufficient magnitude to overcome the capacitance of the membrane of the target cell, facilitating delivery.[24–27] Despite decades of protocol and buffer optimization, adverse effects of electroporation, such as membrane damage, higher anaerobic respiration, decreased ATP availability, oxidative stress, activation of NLRP3 inflammasome leading to proptosis, induction of apoptosis, and even necrosis, remain a concern.[28] As

such, it is critical to advance alternative delivery technologies that can facilitate the manufacturing of emerging CAR-T therapies, with a focus on the health and function of the manufactured product post-process and prior to patient dosing. Previously, we reported a physicochemical transfection system, Solupore, which uses an ethanol-containing delivery solution (DS) with gene editing cargo that can reversibly permeabilize the membrane of target cells.[29,30] Solupore maintains high viability, gene expression homeostasis, and improved efficacy *in vivo* using a CD19 CAR mRNA transfection. In this article, we demonstrate that Solupore can achieve complex gene editing of a lentiviral transduced, cryopreserved product while maintaining high cell viability, higher levels of T_{SCM} CAR-T cells, and improved fitness of the final cell product compared with electroporation, with potential future applications in a rapid manufacturing approach. The outcome is a simulated manufacturing process using a clinical grade Good Manufacturing Practice (GMP)-aligned closed transfection system that yields highly potent CAR-T cells without compromising their regulatory responses and results in a significantly improved product *in vivo*. Currently, there is limited understanding of the cellular consequences of manufactured CAR-T cells. This research offers further insight into T cell function following complex editing and highlights the need to advance manufacturing processes so that cell health is maintained.

RESULTS

Solupore transfection can efficiently deliver complex cargo sequentially to T cells while maintaining high viability and proliferative capacity

As proof of concept that the Solupore transfection process can deliver complex cargo to T cells while maintaining viability, multiplex gene editing using CRISPR-Cas9 ribonucleoproteins (RNPs) was conducted with guide RNAs (gRNAs) targeting TRAC (T cell receptor α constant), B2M (β2 microglobulin), and CD7 (3 μg Cas9/1 × 10^6 cells; 1:2 single guide RNA [sgRNA] molar ratio). Freshly thawed CD3^+ T cells, isolated from leukopaks, were activated via CD3/CD28 for 3 days post-thaw and transfected with RNPs using Solupore. Two Solupore transfection devices were used. The Solupore research tool (RT) is an open, manual device, and the Solupore single-use system (SUS) is an automated and closed clinical SUS. Both Solupore systems performed similarly with TRAC knockout (KO) efficiencies of 73.9% and 73.1%, CD7 KO of 63.7% and 67.5%, and B2M KO of 52.5% and 51.4% for RT and SUS, respectively, across four donors (Figure 1A). Levels of triple KO (TKO) were also comparable at 46.8% and 51.7%, respectively, for RT and SUS. KO efficiencies for each target were also comparable. Individual KO data are displayed in Figure S1 for both Solupore and electroporation (*N* = 4 donors), along with associated recovery percentages.

To determine whether the total number of TKO cells could be increased without compromising cell viability, Solupore and electroporation processes were used to conduct sequential multiplex transfections on the same population of T cells 24 h after the initial transfection. Solupore and electroporation processes demonstrated similar TKO efficiency of 46% for a single multiplex transfection (Figure 1B).

When the sequential multiplex transfection was employed within 24 h, the TKO efficiency following the second Solupore transfection increased from 46% to 70% (Figure 1B), and Solupore demonstrated a 74% increase in the final yield of TKO cells, with the number of live TKO cells increasing from 1.75 × 10^8 to 2.36 × 10^8. When the same study was conducted using electroporation, TKO efficiencies increased from 59% to only 66% following sequential electroporation (Figure 1B). Furthermore, the total number of electroporated TKO live cells decreased by 55% (2.63 × 10^8 to 1.46 × 10^8, representing a loss of transfected cells, reducing the overall yield.

To investigate the contrasting impacts of each transfection method on final cell yield, cell death responses were examined by analyzing membrane integrity and caspase-3 activity of transfected cells at 30 min post-transfection. Cells underwent a single multiplex triple edit of TRAC, CD7, and B2M (hereafter referred to as triple-edited cells) by either Solupore SUS or electroporation transfection. Cells from three donors were used, each carried out in duplicate. The percentage of healthy cells, as determined by live/dead staining, significantly decreased to 80% at 30 min post-electroporation compared with 95% and 92% for untransfected and Solupore-transfected populations, respectively (Figure 1C). More than 15% of cells recovered from electroporation transfection showed signs of early apoptosis, compared to 6% after Solupore transfection (Figure 1C). Late-stage apoptotic cells were identified by measuring the influx of a membrane-impermeable dye into caspase-3 active cells. An additional 9% of electroporation-transfected cells were observed to be in late-stage apoptosis, while only 6% of Solupore-transfected cells were in late-stage apoptosis (Figure 1C). Cumulatively, the overall percentage of apoptotic cells 30 min post-transfection corresponds to 24% for electroporation, compared with 12% for Solupore and 6% for untransfected control T cells across four separate healthy donors.

Transfection processes can affect T cell proliferative capacity and hence cell yield. Following a triple edit by either Solupore or electroporation transfection, T cell proliferation was assessed in three individual donors using 24-well G-Rex bioreactor plates. To account for variations in growth conditions for different processes, proliferation was measured in two different media types, TexMACS and CTSOpTmizer, each supplemented with either interleukin-2 (IL-2) or IL-7 + IL-15. For IL-2-supplemented media, no negative impact was observed in proliferation capacity relative to untransfected control cells for both Solupore and electroporation (Figure 1D). However, a decrease in the proliferation of cells transfected using electroporation was observed in the presence of IL-7 and IL-15 in comparison to IL-2-based stimulation in CTSOpTmizer media, although this was not statistically significant (Figure 1D). This IL-7- and IL-15-associated decrease in proliferation was not as apparent for Solupore or untransfected T cells (Figure 1D).

T_{SCM} retention is enhanced following Solupore

Given the importance of T_{SCM} cells in CAR-T products, this population was assessed via flow cytometry for CD4^+ and CD8^+ triple-edited T cells derived from three healthy donors. This assessment occurred
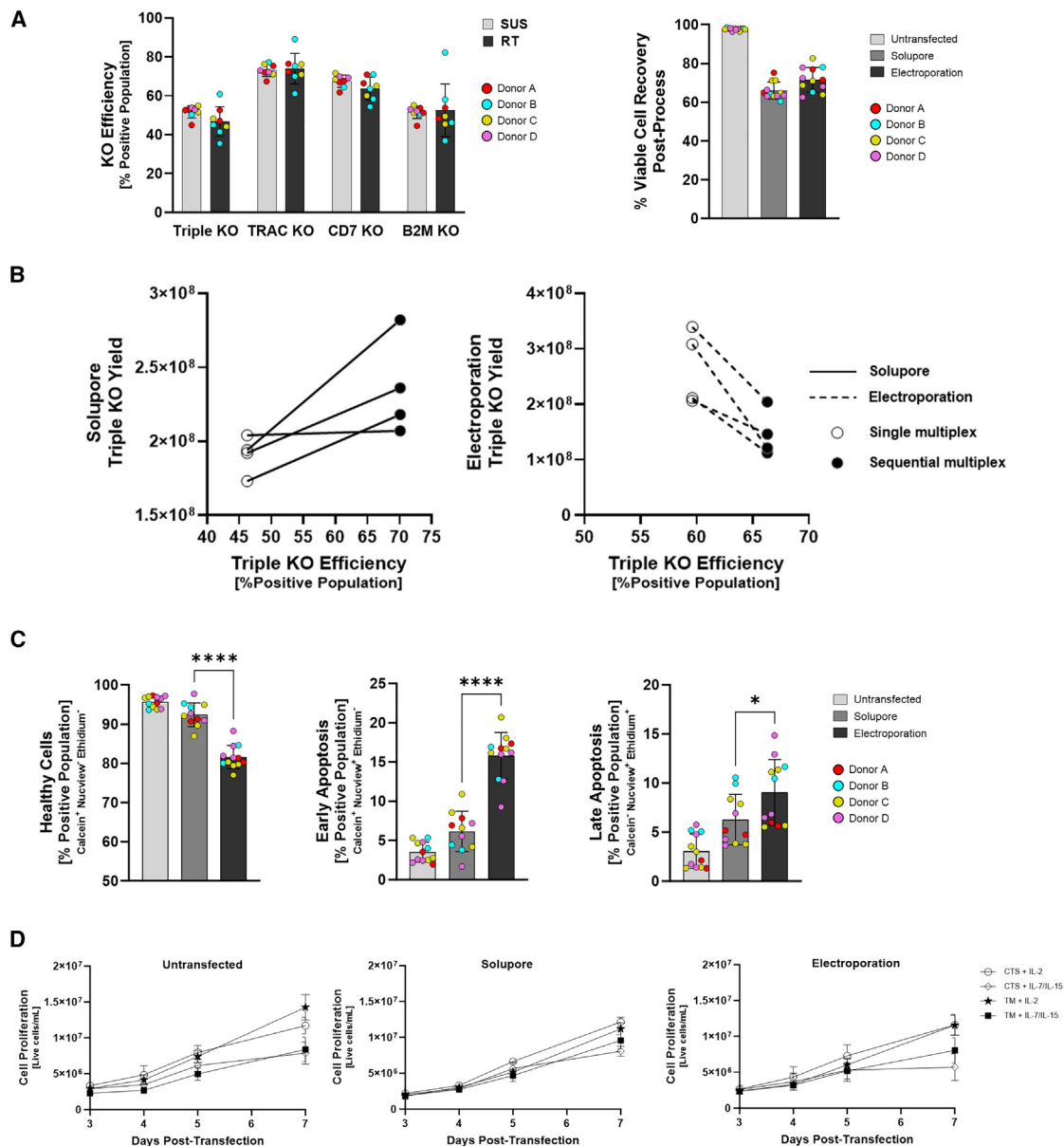
Figure 1. Solupore demonstrates efficient delivery of complex cargo, while maintaining cell expansion and viability

(A) Solupore-based CRISPR-Cas9 RNP KO of TRAC, CD7, and B2M in single transfection of multiplexed guide RNAs (gRNAs) using either the research tool (RT) or the clinical-grade single-use system (SUS), measured 72 h post-transfection. (B) Sequential transfection (a second transfection with multiplexed gRNAs) of the same edited population of cells, examining yield and triple KO (TKO) efficiency following 7 days of proliferation of two independent healthy donors, each in duplicate. Solupore single TKO transfection efficiency = 46.23 ± 1.66, sequential efficiency = 70.10 ± 4.42. Electroporation single TKO transfection efficiency = 59.61 ± 6.42, sequential efficiency = 66.30 ± 1.06. (C) Healthy and apoptotic cells were measured by flow cytometry using a dual-color live/dead stain as well as a caspase-3 activity dye (Nucview-405). Samples were measured 30 min immediately post-transfection using a non-transfected sample as a control for healthy cells from each donor (three donors in duplicate, $n = 6$). Unpaired t test; healthy cells $p < 0.0001$, early apoptosis $p < 0.0001$, and late apoptosis $p = 0.0389$. (D) Untransfected and Solupore- and electroporation-edited cells from $n = 3$ donors were cultured at 1×10^6 cells per well on day 0 in a 24-well G-Rex in either TexMACS or CTSOpTmizer and stimulatory cytokines and expanded for 7 days. Cell counts were performed on days 3, 4, 5, and 7 post-transfection to compare cell proliferation between growth conditions. Data represented as mean +/- SD.

after a single multiplex transfection (day 0) following either the Solupore or the electroporation process. The cells were measured again 4 days post-transfection. On day 0, at 4 h post-transfection, CD4+

T cells had retained 29% of their CD4+ T_{SCM} phenotype after Solupore, compared to 24% after electroporation transfection (Figure 2A). By day 4, both Solupore-transfected and electroporation-transfected cell
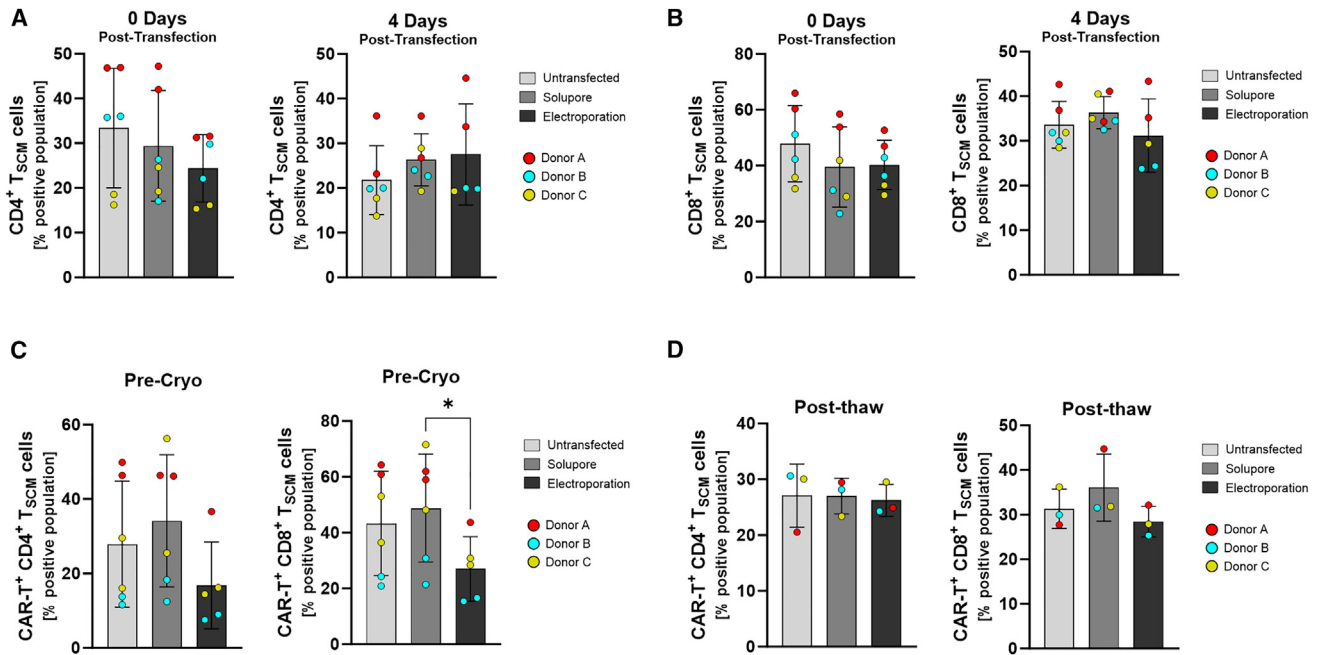
Figure 2. Analysis of TSCM phenotype over time

(A and B) CD4$^+$ (A) and (B) CD8$^+$ T cells were expanded for 0–4 days post-transfection in a 24-well G-Rex plate and stimulation with TransACT and IL-2 (N = 3 donors in duplicate). T$_{SCM}$ phenotype (CD45RA$^+$ CD45RO$^-$ CD62L$^+$ CCR7$^+$ CD95$^+$) was measured by flow cytometry, and a comparison of results for Solupore and electroporation TKO transfected T cells and untransfected control cells is shown. (C and D) CAR-T cells were generated via lentiviral transduction, and the T$_{SCM}$ phenotype of CD4$^+$ and CD8$^+$ CAR-T cells was analyzed 24 h post-transduction (pre-cryopreservation; C) and (D) post-thaw. n = 3 donors, paired t test, p = 0.0396 (C). Data represented as mean +/- SD.

populations consisted of 27% CD4$^+$ T$_{SCM}$ cells (Figure 2A). The CD8$^+$ subpopulation comprised, on average, 40% T$_{SCM}$ cells on day 0 for both processes (Figure 2B). By day 4, 39% of Solupore-transfected cells retained the T$_{SCM}$ phenotype compared with 29% of electroporation-transfected cells (Figure 2B). Two days after transfection, cells were transduced with a lentiviral vector to express CD19 CAR (scFv-41BB-CD3ζ), and the T$_{SCM}$ phenotype of both CD4$^+$/CD8$^+$ T cells was examined 24 h post-transduction. Solupore-transfected CAR-T cells retained 34% CD4$^+$ T$_{SCM}$ cells and 48% CD8$^+$ T$_{SCM}$ cells in contrast to electroporation-transfected cells, which retained only 16% and 26%, respectively (Figure 2C). However, 24 h post-transduction, cells were cryopreserved and T$_{SCM}$ retention was assessed post-thaw, and no significant differences were observed between Solupore and electroporation. CD4$^+$ T cells retained a similar T$_{SCM}$ phenotype across all conditions, including the untransfected control, while for CD8$^+$ T$_{SCM}$ cells, Solupore-transfected cells retained 36% compared with 28% for electroporation-transfected cells (Figure 2D).

Solupore transfection yields metabolically fitter and more functionally responsive T cells

Oxidative phosphorylation within the tricarboxylic acid cycle is associated with a more naive phenotype or T$_{SCM}$-rich population[31] and confers a greater level of effector function upon a metabolic switch to glycolysis for effector T cells.[32–35] Thus, the oxygen consumption rate (OCR) of triple-edited cells from either the Solupore or the electroporation process was examined using the Seahorse analyzer assay.

Transfected cells were cryopreserved 72 h post-transfection, and they were measured 24 h post-thaw. The maximal respiration for Solupore-transfected cells was significantly higher than that of electroporation-transfected cells, with an OCR of 76 pmol/min compared to 53 pmol/min (Figure 3A). The spare respiratory capacity of the overall population of Solupore-transfected cells was 60 pmol/min and for the electroporation-transfected population, it was 41 pmol/min (Figure 3A). For both maximal and spare respiration, the OCR of electroporation-transfected cells was like that of the untransfected control, while for Solupore-transfected cells the OCR was significantly higher for both (Figures 3A and 3B). To determine whether this spare respiratory capacity positively correlated with T cell functionality, cytokine secretion in response to phorbol 12-myristate 13-acetate (PMA) and ionomycin stimulation was examined 4 days post-transfection in a G-Rex 24-well bioreactor. Certain regulatory cytokines such as IL-2, IL-10, and interferon-γ (IFN-γ), were elevated in Solupore triple-edited cells, with IL-2 and IFN-γ being significantly increased for Solupore-transfected cells in comparison to electroporation (Figure 3C). Other cytokines related to cytotoxicity were not differentially expressed based on transfection mechanism (Figure S2). Furthermore, we examined whether the enhanced responsiveness of Solupore-edited cells could be negated by an equally strong feedback inhibition response. We assessed surface expression levels of exhaustion markers in response to repeated stimulation with PMA and ionomycin. Solupore-transfected cells had a significant increase in programmed cell death protein 1 (PD-1) expression (43.41% expression) in response
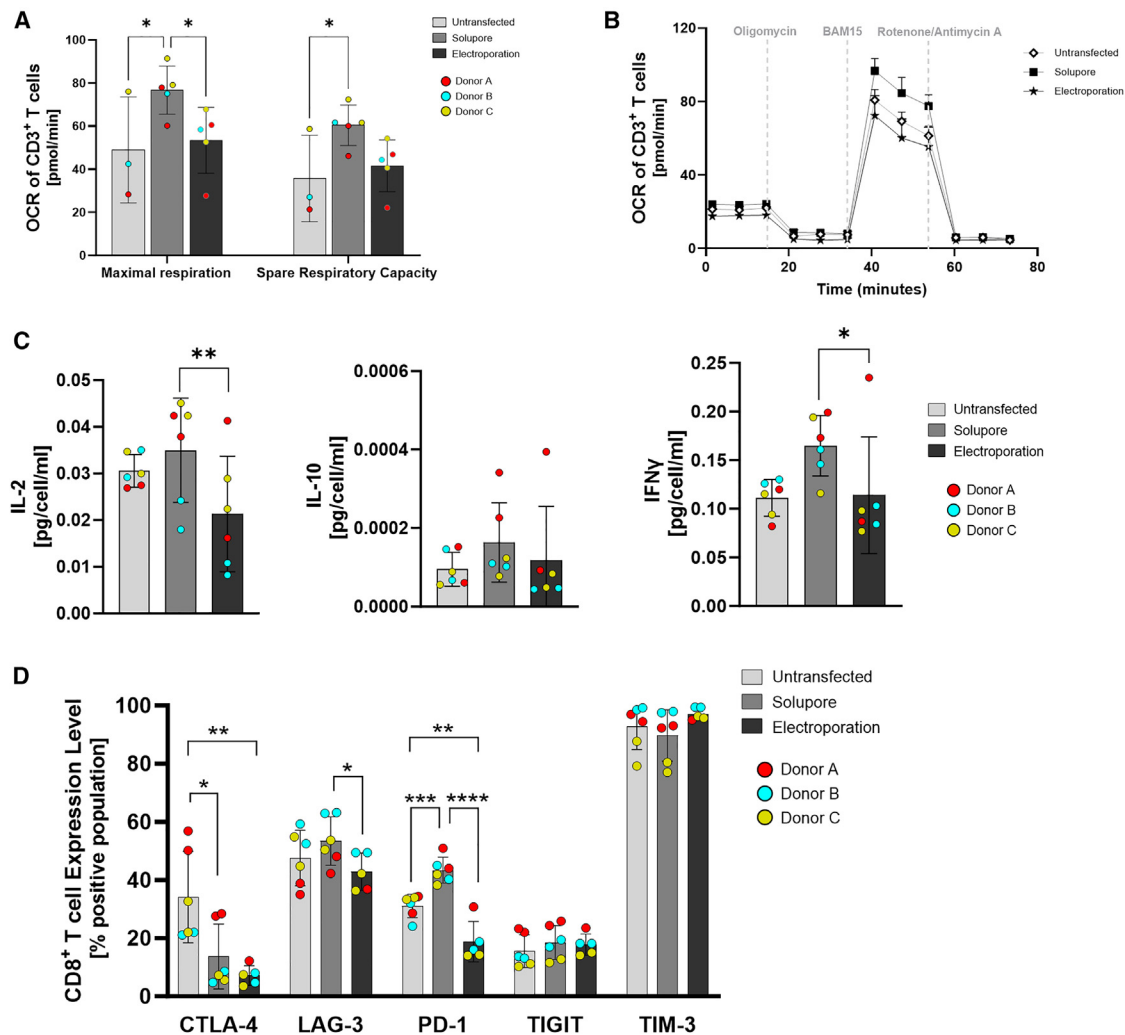
Figure 3. Metabolic health and function of Solupore-transfected cells

(A) Untransfected, Solupore-transfected, or electroporation-transfected cell metabolic potential at 24 h post-thaw (cells were cryopreserved 3 days post-transfection) ($n = 3$ individual donors, two-way ANOVA statistical analysis, $p < 0.05$). (B) Representative OCR profile at 24 h post-thaw. (C) Cytokine profiling 4 days post-transfection. Data were normalized to cell counts on day 4 of the experiment to correlate with relative cytokine production per cell (paired t test, $p = 0.0085$ [IL-2], $p = 0.0498$ [IFN-γ]). (D) Surface marker phenotype data for CD8+ T cells (CTLA-4, LAG-3, PD-1, TIGIT, TIM-3) was 7 days post-transfection after three rounds of stimulation with PMA (10 ng/mL) and ionomycin (250 ng/mL) (stimulation on days 0, 3, and 5 post-transfection). Unpaired t test, untransfected versus Solupore $p = 0.0267$, untransfected versus electroporation $p = 0.0047$ (CTLA-4), Solupore versus electroporation $p = 0.0461$ (LAG-3), untransfected versus Solupore $p = 0.0005$, untransfected versus electroporation $p = 0.005$, Solupore versus electroporation $p < 0.0001$ (PD-1). Data represented as mean +/- SD.

to repeated stimulation (on days 0, 3, and 5) compared to electroporation-transfected cells (18.79% expression) (Figure 3D). Cytotoxic T lymphocyte-associated protein 4 (CTLA-4) was significantly lower for both transfection processes than the untransfected control, in line with CD3/CD28 agonism. Lymphocyte activation gene-3 (LAG-3) expression was increased for Solupore-transfected cells (53.45% expression) in comparison to electroporation (42.87% expression), but only slightly increased compared to untransfected control 47.58%. There were negligible differences in T cell immunoreceptor with immunoglobulin and ITIM domain (TIGIT) and T cell immunoglobulin and mucin domain 3 (TIM-3) across all conditions (Figure 3D).

Solupore transfection improves CAR-T binding and killing of CD19+ cancer cells

The strength of the immunological synapse between a CAR-T cell and a target cancer cell, otherwise known as cellular avidity, has been shown to play an essential role in the effector function of cytotoxic T cells and, ultimately, the efficacy of treatment both pre-clinically and in the clinic.[36–40] We measured cellular avidity on triple-edited CAR-T cells, both pre-cryopreservation and post-thaw. Of samples transduced 48 h prior, the percentage of CAR-T cells bound at a maximum disruptive force of 1,000 pN of force was significantly higher for Solupore triple-edited CAR-T cells in comparison to
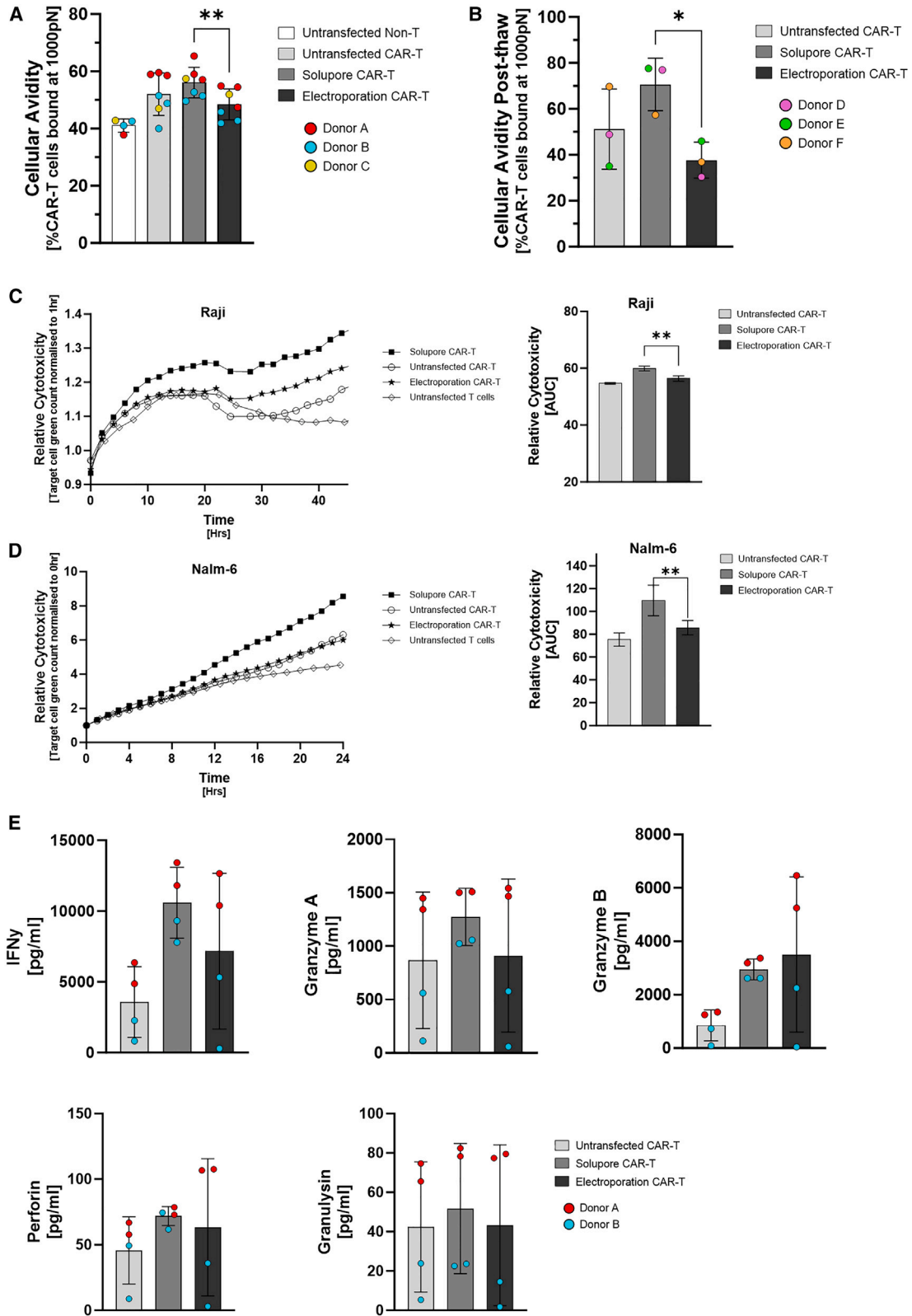
(legend on next page)

electroporation triple-edited CAR-T cells or untransfected CAR-T cells (Figures 4A and 4B). A total of 58% of Solupore triple-edited CAR-T cells remained bound to target Raji cells, in contrast to 49% of electroporation triple-edited CAR-T cells ($p < 0.01$). Furthermore, this difference was greater when samples were cryopreserved and thawed. Solupore triple-edited CAR-T cells showed over 70% of cells remaining bound post-thaw at maximum disruptive force, in comparison to electroporation triple-edited CAR-T cells, which reduced to just over 38%, while 51% of untransfected CAR-T remained bound to the target cells (Figure 4B). This increased cellular avidity was examined as to whether it conferred a more potent cytotoxic effect *in vitro* on Solupore-edited CAR-T cells. CD19$^+$ target Raji and Nalm-6 cells were co-cultured with triple-edited CAR-T cells derived from either Solupore or electroporation triple-edit transfection. Solupore transfection resulted in a cytotoxic profile for both Raji and Nalm-6 cells significantly higher than the electroporation transfection (area under the curve [AUC] $p < 0.01$) (Figures 4C and 4D). Furthermore, key cytokines related to cytotoxicity were quantified when CAR-T cells were co-cultured with Raji cells. The cytokine profile of triple-edited CAR-T cells from Solupore transfection was in line with the enhanced cellular avidity and cytotoxic capacity (Figure 4E).

Solupore transfection results in a significantly more effective CAR-T cell therapy *in vivo*

Triple-edited CAR-T cells were manufactured according to the schematic overview shown in Figure 5A and were dosed in an immunodeficient NOD-*scid* IL2Rgamma^{null} (NSG) mouse model inoculated with Raji-luciferase (Raji-Luc) cells. At 3 days post-inoculation, NSG mice were randomized into groups of eight, within five treatment arms for dosing: PBS vehicle control containing no CAR-T cells, untransfected T cells, untransfected T cells that were transduced to express CD19 CAR (untransfected CAR-T), Solupore triple-edited CAR-T cells, and electroporation triple-edited CAR-T cells. For each group, excluding the PBS control, there were three dosing groups: 1×10^6, 2×10^6, and 4×10^6 cells/mouse. *In vivo* imaging system (IVIS) imaging was conducted over a 25-day period. At the highest dosing group, 4×10^6 cell/mouse, untransfected T cells lacking CD19 CAR were unable to inhibit Raji-Luc cell proliferation and showed similar tumor growth inhibition to the PBS vehicle control, with a total flux of more than 2×10^9 photons per second (p/s) (Figures 5B and 5C). Solupore CAR-T cells, along with untransfected CAR-T cells, caused significantly slower tumor progression in comparison to electroporation-transfected CAR-T cells, which had a tumor progression of 1.72×10^6 p/s on day 4 to 4.48×10^8 p/s on day 25, a 260-fold increase in tumor burden (Figure 5B). The tumor burden was more than 30-fold higher than that found for Solupore

triple-edited CAR-T cells and was extremely statistically significant ($p < 0.0001$) (Figures 5B and 5C). Furthermore, both Solupore-transfected CAR-T cells and untransfected CAR-T cells demonstrated a dose-dependent tumor growth inhibition. Untransfected CAR-T cells demonstrated the most effective tumor growth in both the 1×10^6 and the 2×10^6 dosing arms (Figure 5D). Solupore transfection was comparable to electroporation transfection in the lowest dosing arm, offering little tumor growth inhibition (Figures 5D and 5E). At the 2×10^6 dose, Solupore triple-edited CAR-T cells significantly improved the tumor growth-inhibition capacity in comparison to electroporation triple-edited CAR-T cells. This difference was striking at the highest dose of 4×10^6 cells per mouse. The linearity of the dose response for each treatment arm is demonstrated when each dosing arm at the day 25 time point is graphed together (Figure 5E).

By day 13 of the study, the percentage of engrafted CAR-T cells in the cohort that received Solupore triple-edited CAR-T cells was over 5.4-fold higher ($p < 0.001$) than that observed in the mice group that received electroporation triple-edited CAR-T cells (Figure 6A). To determine whether engraftment or efficacy was influenced by the editing efficiency of the TRAC target, we measured CD3$^-$ cells over time and compared the editing efficiency to tumor burden in each mouse at day 25 (Figures 6B and S3). R^2 analysis suggested no correlation with the KO efficiency of TRAC for Solupore or electroporation-transfected cells. Furthermore, TRAC KO was maintained throughout the study for both Solupore- and electroporation-transfected cells (Figure 6B). The TKO phenotype at terminal endpoint was examined from homogenized spleen tissue, and Solupore triple-edited CAR-T cells were 43% TKO compared with electroporation triple-edited CAR-T cells, which had a 47% TKO (Figures 6C and 6E). Despite poor tumor control by electroporation-transfected cells, the expression of early activation markers for CD4$^+$ T cells was higher in these cells compared to Solupore-transfected and untransfected control cells (Figure 6F). A decrease in CD107a expression occurred in the CD8$^+$ T cell population for electroporation triple-edited CAR-T cells on day 13 from 95% to 70% and at terminal endpoint (day 26) from 93% to 66% (Figure 6G). This reduction in CD107a expression on days 13 and 26 correlates with an increase in the exhaustion marker PD-1 (Figure 6H). Expression of PD-1 in electroporation-transfected cells was elevated compared to untransfected and Solupore-transfected cells on days 13, 18, and 26, reaching over 64% of CD8$^+$ T cells, 2-fold higher than Solupore-treated cells (Figure 6H).

DISCUSSION
For difficult-to-treat hematological malignancies such r/r chronic lymphocytic leukemia (CLL) or r/r MM, it is important to improve

---

Figure 4. Comparison of effector function of CAR-T product generated from Solupore and electroporation triple-edited T cells

(A and B) Cellular avidity was measured using the z-Movi and is represented as percentage of cells bound to target cells after a maximal force of 1,000 pN has been applied ($n = 3$ donors; donors A–C were used for [A], while donors D–F were used for [B]). Paired t test, $p = 0.001$ (A), 0.0486 (B). (C and D) Raji and Nalm-6 cells (CD19$^+$) co-culture with triple-edited and cryopreserved T cells (CD19 CAR$^+$). Cytotoxicity was measured using the Incucyte S3 Live-Cell Analysis System for 48 h. Representative figure for 1:1 ratio (Raji) and 4:1 ratio (Nalm-6); $n = 3$ (mean of three donors). AUC analysis was performed to compare the differences between sample cytotoxicity (unpaired t test, $p = 0.0089$ [C], 0.0015 [D]). (E) Cytokine profiling from supernatants of a 1:1 co-culture between Raji cells and untransfected, Solupore, and electroporation CAR-T cells. Supernatants were harvested 24 h post-co-culture. Data represented as mean +/- SD.

A

B

C

D
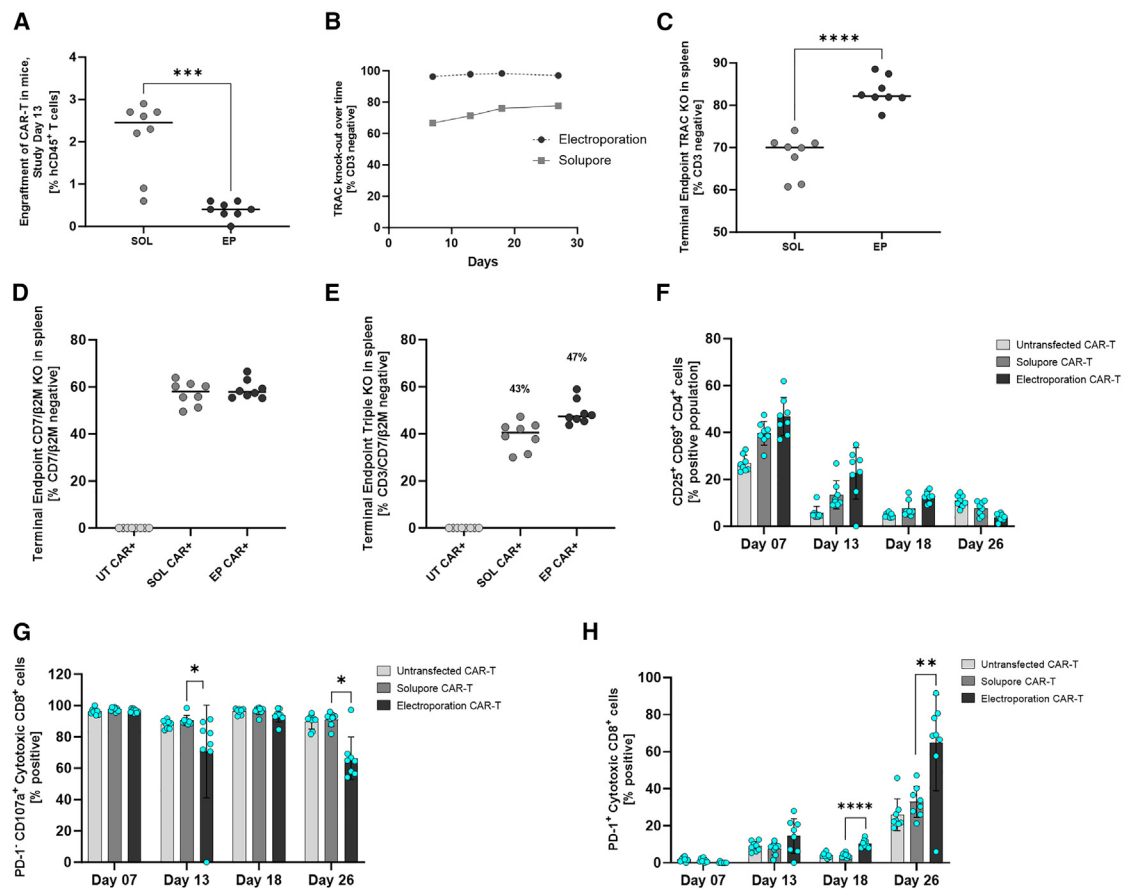

E
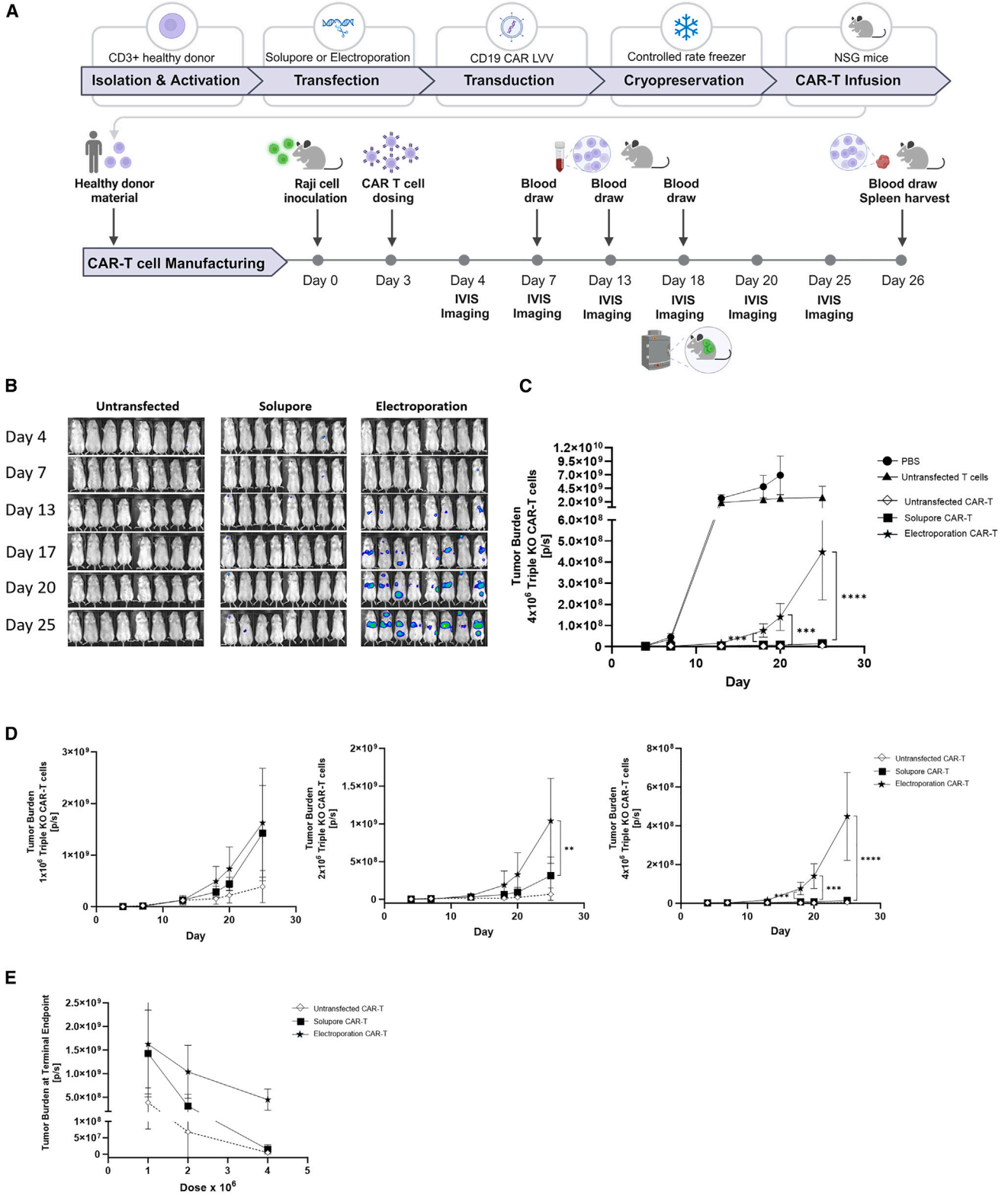
(legend on next page)

Figure 6. *In vivo* study analysis of cell product engraftment and activation

Flow cytometry analysis of blood draws from mice on study days 7, 13, 18, and 26 (A, B, and F–H) or homogenized spleens at the study endpoint (day 26, C–E). (A) The percentage of engrafted CAR-T cells in mice based on human CD45-expressing (B and C) KO of TRAC across untransfected (UT), Solupore (SOL), and electroporation (EP) groups by flow cytometry. unpaired T-test $p = 0.0008$ (A) and unpaired T-test $p <0.0001$ (C). (D and E) TKO quantification from homogenized spleen cells. (F) Early activation marker quantification by expression of the surface markers CD25 and CD69. (G and H) Cytotoxic populations determined by expression of CD8+ CD107a+ T cells (G) Mann-Whiteny test $p = 0.0281$ and exhaustion assessed by expression of PD-1 (H) unpaired T-test $p <0.0001$ Day 18. $p = 0.0051$ Day 26. Data represented as mean +/- SD.

next-generation CAR-T therapies to overcome current shortcomings.[41] Of equal importance is to increase understanding of the complexities of manufacturing processes and their impact on cell product function. By defining critical quality attributes (CQAs) of cell therapeutic products, next-generation manufacturing using complex gene editing processes can be improved to maximize product quality and potency and thus improve clinical success. T cells are complex[42]; hence, understanding the impact that manufacturing processes have on these cell products is vital to advance the development of adoptive cell therapies.

We have simulated the manufacturing of a complex edited CAR-T product and investigated several important attributes related to T cell health and function. We used a GMP-compliant, clinical non-viral, closed transfection system, Solupore,[29,30] benchmarked against a current non-viral standard transfection process, the impact of which is not completely understood for CAR-T cells.[43] Previously, Solupore-transfected cells demonstrated improved *in vivo* efficacy using a CAR mRNA transfection in comparison to a non-viral standard control. Here, we have generated a triple-edited, cryopreserved CAR-T cell product and investigated specific properties related to

Figure 5. Tumor growth analysis in NSG mice inoculated with CD19+ Raji-LUC cells measured over 25 days

(A and B) IVIS imaging and tumor burden measurement using luminescent target Raji cells expressing CD19 (Raji-LUC) in an NSG mouse model over 26 days ($n = 8$), comparing Solupore TKO CAR-T cells with untransfected CAR-T cells, untransfected cells (negative for CAR), electroporation CAR-T cells, and PBS/vehicle control. (C–E) Dose-dependent response of Solupore TKO CAR-T cells, untransfected CAR-T cells, and electroporated TKO CAR-T cells. (D) Day 18 Welch's t test, $p = 0.0005$, day 25 unpaired t test, $p < 0.0001$. 2×10^6 day 25 $p = 0.0088$; 4×10^6 day 13 Mann-Whitney, $p = 0.003$; day 18 Welch's t test, $p = 0.0005$; day 25 unpaired t test, $p < 0.0001$. Data represented as mean +/- SD.

T cell functionality following a thaw cycle. The potential importance of specific CQAs of T cells, such as OCR and cellular avidity, in complex editing processes is underscored when comparing Solupore and electroporation transfection processes. It is well understood that electroporation is stressful to cells[28]; this is even more notable when comparing sequential electroporation processes on a population of cells, as shown in Figure 1B. A second consecutive transfection, if not toxic or stressful to cells, should increase the overall yield and editing efficiency. The observed increase in yield after Solupore transfection suggests that it is a non-toxic, non-stressful process for cells, further supported by a higher proportion of healthy cells and a lower proportion of cells in apoptosis compared with electroporated cells (Figure 1C). Sequential multiplex transfection using electroporation effected a limited increase in yield of only 3.5%, in contrast to sequential multiplex Solupore transfection, which yielded 86% more triple-edited cells. Interestingly, despite higher caspase-3 activity and a 2-fold increase in apoptotic cells, electroporation-transfected T cells were observed to proliferate in a trend similar to that of untransfected T cells and Solupore-transfected T cells. It is possible that the apoptotic or necrotic response to electroporation, as shown in Figure 1C, stimulates stress response pathways and inflammatory signal transduction pathways. These pathways could act as pro-survival signals to aid in proliferation responses, for example, through the detection of extracellular ATP.[44–47] Apoptotic response and genome-wide dysregulation after electroporation has been previously reported compared to Solupore,[29] and we hypothesize that unregulated inflammatory signal transduction responses could occur immediately post-electroporation to drive or prime T cells from a naive phenotype or T_{SCM} cells into a more mature effector state.[17,48,49] Indeed, when transfecting naive T cells with mock cargo (buffer alone), early activation markers are detected for electroporation transfection but not for Solupore transfection (Figure S4).

Further to this, no significant drop in the retention of T_{SCM} cells after Solupore transfection was observed, with similar profiles of T_{SCM} cell retention of untransfected control cells as well as electroporation (Figures 2A–2D). Solupore did not adversely affect the T_{SCM} population here, and a similar result was seen in genetic profiling by Kavanagh et al.[29] (no adverse reaction for gene transcription). Thus, it is reasonable to assume that the Solupore physicochemical transfection process minimally perturbs signal transduction and genetic regulation of target cells, maintaining homeostasis and a naive status, similar to untransfected cells throughout the manufacturing process. It is well understood that higher numbers of CAR T_{SCM} cells confer an enhanced response in the clinic; thus, manufacturing processes that promote the maintenance and retention of this subpopulation are preferred. For the purpose of producing a high proportion of CAR$^+$ cells, we included a lentiviral transduction step to support *in vitro* experiments so that functional characterization could be achieved following target gene KO. As gene-modifying strategies improve, a completely non-viral product will be preferable. In this article, we have demonstrated that following a triple edit and a transduction step, there is a significantly higher percentage of CAR T_{SCM} cells post-Solupore treatment than electroporation, and this advantage is maintained even after cryopreservation and thawing (Figure 2D). Interestingly, this effect was less consistent in CD4 T_{SCM} cells compared to CD8 cells from the same donors from days 0 to 4 and including thawed cryopreserved cells because there was no significant difference between pre-cryopreserved cells and post-thaw cells for Solupore transfection and electroporation (Figure 2C). However, there is a noticeable trend, with the exception of donor A, which retained a high T_{SCM} phenotype for electroporation transfection. It is likely that more donors would provide a more consistent and statistically significant insight between CD4/CD8 cells.

In addition to T_{SCM} retention, cellular metabolism has become an increasingly important facet of immune function[50–53] and, by extension, could be an essential attribute in CAR-T cell manufacturing for clinical use.[54] On examination of the temporal dynamics of oxidative phosphorylation (OXPHOS; as measured by OCR; Figures 3A and 3B), a higher spare respiratory capacity within the manufacturing process, after Solupore transfection, was observed. This higher spare respiratory capacity confirms the enhanced retention of naive-like T cells and is correlated with greater levels of cytokines released for a subset of key cytokines (Figure 2C). Spare respiratory capacity may not only confer a simple increase in cytokine release but also has been reported to shape downstream immune responses on a systemic level, besides having a significant role in the regulation of T cell activation and exhaustion.[55] Metabolic dysregulation has been demonstrated to precede T cell exhaustion.[56] However, when analyzing the PD-1 expression in Solupore-transfected cells in response to repeated stimulation, higher PD-1 expression correlated with higher OXPHOS. Coupled with the maintenance of genetic homeostasis and lack of perturbation on cell health by Solupore transfection, this suggests that the increase in PD-1 is a healthy regulated response to repeated stimulation rather than uncontrolled excess-inflammatory responses (Figure 3D).

It has been demonstrated that following T cell activation, there is a poor correlation between RNA expression dynamics and the level of encoded proteins.[57,58] This suggests that the majority of proteome regulation post-activation is post-transcriptional regulation.[34] Therefore, with CAR expression 3 days post-activation and 2 days post-transfection (5 days total post-transfection process), it is possible that the post-transcriptional regulation of activated T cells is impacting cellular avidity. Measured cell avidity in T cells following electroporation transfection is comparable to untransfected T cells but is significantly lower in comparison to Solupore-transfected T cells (Figures 4A and 4B), suggesting that Solupore transfection is potentially altering post-transcriptional regulation in a positive manner in comparison to untransfected control. Further investigation is required to understand this possible impact on proteomic regulation in cell therapy manufacturing. Nonetheless, on examination of the killing of CD19$^+$ Raji and Nalm-6 cells by triple-edited CAR-T cells (Figures 4C and 4D), the downstream impact is clear: higher targeted and potent cytotoxicity of Solupore-transfected T cells compared to electroporation-transfected T cells, which is the primary goal of manufactured CAR-T products. The measured cytotoxic potency of the Solupore-transfected T cells is supported by the measured levels of

cytolysis-specific cytokines, associated with CD8$^+$ cells, which show a similar trend for Solupore-transfected versus electroporation-transfected T cells (Figure 4E).

To determine whether the *in vitro* data described thus far are reflective of an improved manufactured product, triple-edited CAR-T cells were dosed in immunodeficient mice inoculated with CD19$^+$ Raji cells (schematic overview, Figure 5A). The difference in response is striking: Solupore triple-edited CAR-T cells limited tumor progression in a manner that was comparable to that of untransfected CAR-T cells, while electroporation-transfected CAR-T cells failed to inhibit tumor progression, resulting in a statistically significant 30-fold improvement in efficacy in the 4×10^6 cell dose groups (Figures 5B and 5C). Furthermore, Solupore transfection demonstrated a dose-dependent protection against tumor growth, an effect that was not prominent for electroporation (Figures 5C and 5D). Interestingly, untransfected control CAR-T cells had an improved tumor growth inhibition profile compared with Solupore-transfected CAR-T cells, although measured spare respiratory capacity, cellular avidity, and cellular cytotoxicity in Solupore triple-edited CAR-T cells were higher than in untransfected CAR-T cells (Figures 3A, 4A, 4C, and 4D). It is thus important to note the unique qualities of individual donors. In this research article, donor C, examined in the cell avidity assay of cryopreserved cells (Figure 4B), was the same donor used in the manufacturing process described in Figure 5A, and presented in the *in vivo* datasets in Figures 5 and 6. In donor C, untransfected CAR-T cells showed improved cellular avidity compared to Solupore-transfected CAR-T cells, which translated to improved efficacy *in vivo*. These data support suggestions in the recent literature that cell avidity is predictive in preclinical modeling of CAR-T efficacy.[36–40] However, with only a single donor to compare, it is important that further work is done on the predictive power of cell avidity in terms of *in vivo* efficacy. Conversely to cellular avidity, cytokine profiling of CD19-mediated activation of CAR-T cells in this study appeared to act as a poor predictor of *in vivo* efficacy, which is inconsistent with PMA/ionomycin-mediated activation of T cells, a non-specific mode of activation. Overall, this is in line with a recent study carried out by Leick et al., which investigated functional *in vitro* assays and correlated them with tumor burden reduction *in vivo* and found that cytokine profiling did not correlate well with *in vivo* performance.[36]

Interestingly, despite surface marker expression of early signs of activation after electroporation transfection (CD4$^+$ CD25$^+$ CD69$^+$ T cells and CD8$^+$ CD107a$^+$ T cells) in the mouse model, limited efficacy was observed (Figures 6F and 6G). This limited efficacy may be due to the potentially longer-lasting adverse attributes of cells processed by electroporation discussed previously, and it may be partially due to the early onset of exhaustion observed. That said, by day 26 of the study, the tumor burden was reaching the upper limit for electroporation-transfected CAR-T cells, and it is therefore unsurprising that the PD-1 expression is above 60% in this treatment group compared to groups with limited tumor progression. Furthermore, the increase in PD-1 expression in electroporation-transfected CAR-T cells

observed on day 13 of the study was not consistent across all mice in the group, and by day 18, the increase in PD-1 relative to Solupore-transfected and untransfected CAR-T cells was only a small fraction of the entire population (mean of 10.4%; Figure 6H). Therefore, PD-1 expression cannot account for the limited efficacy in the mice. Similarly, a correlation of TRAC KO efficiency and tumor burden reduction was examined to understand whether the higher capacity to control tumor growth was associated with lower TRAC KO of Solupore-transfected cells. No consistent correlation between KO efficiency and tumor control was found (correlation coefficient of −0.45 for Solupore transfection, 0.6 for electroporation) (Figure S3). This suggests that CD3 expression has a limited capacity to influence CD19$^+$ Raji cell growth *in vivo* in this NSG mouse model and that the majority of the cytotoxicity effect on tumor control is primarily driven by CD19 CAR expression, as further demonstrated by untransfected T cells (CD19 CAR$^−$) and untransfected CAR$^+$ control arms (Figure 6B). Aside from TRAC KO efficiency and PD-1 expression, phenotypically, Solupore CAR-T cells and electroporation CAR-T cells are relatively equal in terms of activation markers, aside from the noted difference in the CD8$^+$ CD107a$^+$ subpopulation. Currently, transfection technology may not succeed in the generation of >90% population carrying the phenotype of interest, as is the case in the murine study (Figure 6E). However, the TKO phenotype is limited due to the difficulty of achieving high efficiency for the B2M gene for both Solupore and electroporation, limiting the overall TKO efficiency. KO efficiency can be optimized, and as discussed above for TRAC, appeared to have no impact on tumor burden reduction (Figure S3). Furthermore, the edited cell treatment arms at 1e6 and 2e6 cells per mouse, including Solupore transfection, performed worse overall in terms of *in vivo* control of tumor growth (Figure 6D), which calls into question the benefit of multi-edited CAR-T cells as opposed to standard CAR-T cells. While not the purpose of this study, multi-edited CAR-T cells are expected to improve or overcome current hindrances in cell therapies. For example, allogeneic cell therapy could overcome current quality control (QC) limitations on cell product manufacturing, as well as other benefits, but would require multi-editing to render the products safe from the effects of graft-versus-host disease. As cell therapy development improves, multi-editing CAR-T cells to control solid tumors could become an attractive treatment option.[59]

In summary, when comparing two non-viral GMP transfection processes and assessing the health and function of those cell products, the most striking differences between the two cell populations, other than transfection mechanism, is T$_{SCM}$ subpopulation retention post-process, which is associated with a higher OXPHOS, and the cellular avidity of CAR-T cells bound to CD19$^+$ Raji cells. Taken together, these attributes confer enhanced cytotoxicity potential and a more efficacious, potent, and durable response *in vivo*. As CAR-T products become more refined through genetic modification to improve efficacy, manufacturing processes will increase in complexity. The development and optimization of manufacturing processes using novel, non-viral technologies like Solupore that foster CQAs of cell health and function could lead to greater therapeutic success in the clinic.

Non-viral transfection technologies that support more complex and rapid manufacturing of potent cell products for application in difficult-to-treat malignancies, such as r/rCLL or r/rMM, can ultimately improve complete remission rates. In this study, we showed that Solupore can produce healthier and more functional cells compared to cells modified with nucleofection. Nucleofection has been widely adopted as a gene editing delivery platform that utilizes both gentle and higher efficiency settings (programs EO115 and EO117, respectively); similarly, MaxCyte has a high- and low-energy setting to allow the developer to choose either higher-modification efficiencies or higher-modification viabilities. Lastly, Thermo Fisher/CTS Xenon also offers flexibility to programmatically change the electrical pulse energy settings applied to the cells. Solupore is among a number of emerging non-viral delivery technologies developed to modify cells more gently and efficiently for clinical applications that do not rely solely on electroporation as their delivery mechanism. These technologies include CellFE and Kytopen, which utilize microfluidic mechanoporation and electro-mechanoporation mechanisms, respectively. In contrast, Solupore uses a physicochemical mechanism that we compared with the EO115 nucleofection "gentle" transfection setting in this study. Solupore technology advantages include excellent *in vivo* CD19 CAR-mediated cytotoxicity, enablement of sequential transfections, and efficient use of reagents in GMP workflows. Disadvantages include the relatively narrow range of cell types for which comprehensive datasets have been developed, with a current application focus on T cells. Future work in this field should include broadening the applicability of this technology to other cell types and manufacturing workflows. Based on the data presented in this research article, optimizing cell health in gene-editing manufacturing processes has the potential to improve CAR-T products and support the manufacture of next-generation cell therapy products.

MATERIALS AND METHODS
Ethics
All experimental methods were carried out in accordance with the approved guidelines. All gene editing work was carried out under the Environmental Protection Agency licenses G0684-01 and G0733-01. Leukopaks from healthy donors were sourced from BioIVT in full compliance with Good Clinical Practice as defined under FDA and US Department of Health and Human Services regulations and International Council for Harmonization of Technical Requirements for Pharmaceuticals for Human Use guidelines. The murine CAR-T cell efficacy study was performed at The Jackson Laboratory, an AAALAC (Association for Assessment and Accreditation of Laboratory Animal Care) International-accredited and Office of Laboratory Animal Welfare-assured institution. The Jackson Laboratory adheres to all applicable international, national, and institutional policies for the care and use of research animals. All experiments were approved by the Institutional Animal Care and Use Committee of The Jackson Laboratory.

Isolation of primary human T cells
Leukopaks (BioIVT, HUMANLMX100-0001129) were obtained from de-identified and healthy human donors. T cells were isolated from the fresh Leukopak, within 24 h of collection, via positive selection using the Straight from Leukopak CD4 (Miltenyi Biotec, 130117022) and CD8 (Miltenyi Biotec, 130117019) Microbead kits and MultiMACS Cell24 Separator Plus (Miltenyi Biotec 130-098-637), according to the manufacturer's protocol. Briefly, CD4/CD8-labeled Leukopak samples were loaded onto the Multi-24 Column Block (Miltenyi Biotec, 130-095-692), where, after removing the column block from the magnetic field, the magnetically retained $CD4^+$/$CD8^+$ T cells were eluted as a positively selected cell fraction. Purified T cells were resuspended in CryoStor CS10 (STEMCELL Technologies, 07930) to achieve the desired density for cryopreservation and transferred to labeled cryovials. Cells were frozen using a controlled rate freezer (CRF; Thermo Fisher Scientific Cryomed) and stored in a $-150^{\circ}C$ freezer until required.

Culture and preparation of T cells for experimental use
T cells were thawed using a $37^{\circ}C$ bead bath and activated at a cell density of 1×10^6 cells/mL in complete TexMACS media (Miltenyi Biotec, 130-097-196) containing 5% Human AB Serum (Bio IVT HUMANABSRMP-1), 120 IU/mL human IL-2 (Cellgenix, 1020-050 or Bio-Techne, BT-002-AFL-050), and activated using TransAct (Miltenyi Biotec 130-111-160) at a final concentration of 10 μL/1×10^6 cells. T cells were left undisturbed for 72 h in an incubator at $37^{\circ}C$, 5% CO_2, and 20% O_2. At 72 h post-activation, T cells were visually inspected before QC analysis. QC release criteria was >85% viability, $\geq$90% for $CD3^+$ (Thermo Fisher Scientific, 17-0037-42), and >80% for $CD25^+$ (Miltenyi Biotec, 130-113-286) by flow cytometry (Novocyte 3000, Agilent). Cells were centrifuged at 350 relative centrifugal force (rcf) for 7 min (at room temperature, acceleration 9, deceleration 9). The cell pellet was resuspended in basal TexMACS media (without serum or IL-2) and counted using a Via-1 cassette (Chemometec, 941-0012). A master mix of cells was then prepared for the required transfection method or assay and verified for accurate cell density. For any required untreated cell conditions, 12×10^6 cells in 24 mL complete TexMACS media were seeded into a T75 tissue culture flask (Sarstedt, 83.3911.002).

Cell lines
All cell lines (Jurkat, Jurkat FMC, Nalm-6, and Raji) were originally obtained from the American Type Culture Collection. Cells were expanded in RPMI medium containing 10% fetal bovine serum (FBS) maintained at a density of $<2 \times 10^6$ cells/mL and kept at a low passage. Jurkats and Jurkats FMC media were also supplemented with 1% L-glutamine 200 mM (Thermo Fisher, 25030081) and 0.1% v/v β-mercaptoethanol (Gibco, 21985-023). All cells were cultured in standard conditions using a humidified incubator with set points $37^{\circ}C$, 5% CO_2, and 20% O_2.

RNP formulation for gene editing
To transfect 20×10^6 cells, 366 pmol Alt-R S.p. HiFi Cas9 Nuclease V3 (IDT, 10007803) was combined with 732 pmol sgRNA (IDT; targeting either TRAC [AGAGTCTCTCAGCTGGTACA], B2M [GGCCGAGATGTCTCGCTCCG], or CD7 [GGAGCAGGTGATGTTGACGG]) and incubated at room temperature for 10 min (dose of

Table 1. Delivery solution and cargo preparation

Delivery solution constituents	Volume, μL
WFI	7.488
SA Buffer (stock 20×; final 1×)	4
Ethanol (stock 100%; final 5%)	4
Cas9 RNP (TRAC)	21.5
Cas9 RNP (CD7)	21.5
Cas9 RNP (B2M)	21.5
Total	80

each RNP: 3 μg Cas9/1 $\times$ 10^6 cells at 1:2 Cas9:sgRNA molar ratio). Prior to use, the RNP preparation was stored at 4°C.

Solupore transfection
This method describes the clinical-scale Solupore-transfection process using the automated, closed, non-viral transfection platform Solupore SUS (Avectas). Cargoes of required concentration were combined with Solupore delivery solution (DS), which consists of Solupore SA Buffer (Avectas, A-AVE103-0001-01), Solupore Ethanol (Avectas, A-AVE103-0004-01), and water for injection (WFI; Fisher Scientific, 10317002) for a final 80 μL total transfection volume (Table 1).

Once the cargo was prepared, it was aseptically loaded into the single-use assembly (SUA) reservoir at a concentration of 7.4 μM Cas9 with 14.9 μM sgRNA per target per transfection. The target T cells (72 h post-activation, 20 $\times$ 10^6 cells/30 mL of basal TexMACS media per transfection) and transfection solutions (complete TexMACS media) were added to transfer bags and sterile welded to the SUA as per the manufacturer's protocol. Following the manufacturer's protocol, the SUA was loaded onto the multi-use controller (MUC), and a protocol was selected for T cell CRISPR RNP transfection. In brief, the MUC control system was used to atomize the cargo, deliver it to cells, and recover the cells from the SUA. Solupore's physicochemical process was used to deliver cargo to T cells 72 h post-activation with TransAct and IL-2. The cargo was prepared in DS with 5% v/v ethanol and placed in the reservoir of the SUA. In an automated procedure, 20 $\times$ 10^6 T cells in 30 mL basal media were pumped into the SUA chamber. The media was removed, transiently exposing the cells on the SUA chamber filter membrane. The Solupore spray was then actuated, allowing temporary permeabilization of the cell membrane and facilitating the entry of cargo. The cells were then resuspended in 5 mL complete TexMACS media, and after a short 30-s incubation, cells were resuspended in an additional 25 mL TexMACS media and extracted from the SUA chamber into a harvest bag for recovery into a T-Flask in a final total volume of 30 mL cell culture media. The recovered cells were counted using a Via-1 cassette on the NC200, samples were taken for post-transfection analysis, and the remaining cells transferred to the required culture vessel (T75 flask or G-Rex) and placed in a humidified incubator with set points 37°C, 5% CO_2, and 20% O_2. Cells were expanded using TexMACS or CTSOpTmizer media containing 120 IU/mL IL-2 or 5 ng/mL IL-7

(Bio-Techne, BT-007-AFL-025) and 2.5 ng/mL IL-15 (Bio-Techne, BT-015-AFL-025).

Transfection using electroporation
Cells were electroporated with the 4D-Nucleofector system (Lonza Bioscience) using the 100-μL Nucleocuvette format as per the manufacturer's protocol with the P3 primary cell 4D-Nucleofector X kit L (Lonza, V4XP-3024). As recommended by the manufacturer for human T cells, 20 $\times$ 10^6 T cells (72 h post-activation) were centrifuged at 350 rcf for 5 min, supernatant media removed, and cells resuspended in 800 μL PBS and divided into four 1.5-mL microfuge tubes as 200 μL aliquots of 5 $\times$ 10^6 T cells each. Samples were centrifuged at 200 rcf for 5 min, and each pellet was resuspended in room temperature-supplemented Nucleofector P3 buffer and gently pipetted onto the RNP cargo, to a total volume of 100 μL. The cell and cargo suspension in each tube was transferred to four separate nucleocuvettes and electroporated with pulse code EO-115 in the 4D-Nucleofector X unit. The nucleocuvettes were returned to the biosafety cabinet (BSC), and the supplied pipette was used to add approximately 500 μL of 37°C complete media to each cuvette and to pool the contents of the four nucleocuvettes into the same T75 recovery flask. Samples were harvested for cell counting using a Via-1 cassette on the NC200.

Assessment of transfection efficiency
Assessment of transfection KO efficiency of TRAC, B2M, and CD7 was carried out by flow cytometry staining with a master mix of anti-CD3 (BioLegend, 344816), anti-histocompatibility leukocyte antigen (HLA) (BioLegend, 311410), and anti-CD7 (BioLegend, 343104), respectively. A sample of 1 $\times$ 10^5 cells was harvested on day 4 post-transfection, washed once in fluorescence-activated cell sorting (FACS) buffer (PBS, +0.5% FBS), and resuspended in the antibody master mix for 10 min in the dark at room temperature. Cells were washed once, centrifuged, and resuspended in 100 μL FACS buffer for acquisition on a Novocyte 3000 flow cytometer. For analysis, live cells were gated using Zombie Violet vital dye exclusion (BioLegend, 423113), and %KO was analyzed using NovoExpress software (version 1.6.1). Untransfected control cells were used to establish gates by staining with Fluorescence Minus One (FMO) controls for each specific marker.

Transduction with CD19 CAR lentiviral vector
Transduction of CD3$^+$ T cells was carried out 48 h post-Solupore or electroporation transfection. Transduction was carried out in 96-well plates or 6-well plates coated overnight in 5 μg/mL retronectin in PBS. CD3$^+$ T cells were plated at 1 $\times$ 10^6 cells/mL in complete TexMACS containing anti-CD19 CAR lentivirus (scFv-41BB-CD3ζ, 104882); Creative Biolabs, VP-CAR-LC633) at required MOI with 50 μM deoxynucleotide triphosphates (Brennan & Company, N0447S). For transductions in 6-well plates, plates were centrifuged at 700 rcf for 90 min at room temperature. Plates were then placed into a 37°C incubator at 5% CO_2 and 20% O_2 for 24 h. The efficiency of transduction was measured by evaluating viable CAR expressing cells by flow cytometry. A total of 2 $\times$ 10^4 cells were sampled from wells

and stained with biotin-conjugated CD19 CAR Detection Reagent (Miltenyi Biotec, 130-129-550), according to the manufacturer's instructions, and prepared in CAR detection buffer (0.5 M EDTA, 7.5% BSA in PBS) for 10 min in the dark at room temperature. Cells were washed in detection buffer, centrifuged, and resuspended in secondary anti-biotin phycoerythrin (PE) (Miltenyi Biotec, 130-110-951), also prepared in detection buffer, for 10 min in the dark at room temperature. Cells were washed in detection buffer, centrifuged, and re-suspended in 100 μL detection buffer with 1:40 7-aminoactinomycin D (7-AAD) viability dye (Miltenyi Biotec, 130-111-568). Samples were acquired on a Novocyte 3000 flow cytometer, and untransfected non-transduced cells were used to set gates for viable %CAR$^+$ expression.

Cryopreservation of CAR-T cells

Transfected, transduced CAR-T cells were harvested for cryopreservation 24 or 48 h post-transduction. Where required, samples were pooled post-harvest and weighed to accurately determine the volume of cells. A cell count was performed as previously described and total viable cells calculated. Samples were centrifuged at 350 rcf for 5 min. Supernatant was removed, and pellets were resuspended in CryoStor CS10 (STEMCELL Technologies, 07930) to achieve the desired density for cryopreservation and transferred to labeled cryovials. Preliminary studies were carried out by freezing T cells at a density of 2×10^6 cells/mL. Following subsequent analysis, an optimal density of 4×10^6 cells/mL was identified. Samples were frozen using the CRF operated on the T cell program according to the manufacturer's guidelines. In brief, samples in cryovials were added to the CRF once it had cooled to 4°C, and the temperature probe was placed in close contact with the cryovials. Upon completion of a freezer run, samples were immediately transferred to the −150°C freezer for storage until required.

For freezing cells in Mr. Frosty (MRF; Nalgene 5100-0001), samples were centrifuged at 350 rcf for 5 min and resuspended in CryoStor at a density of 2×10^6 cells/mL, aliquoted into 2-mL cryovials, and placed in a room temperature MRF. After the addition of cryovials, MRF was transferred to a −80°C freezer to cryopreserve cells at a rate of −1 °C/min. After 24 h, the MRF was retrieved from a −80°C freezer, and the vials were stored at −150°C until required.

Flow cytometry for T cell phenotyping

Flow cytometry (Novocyte 3000) was utilized to examine the T_{SCM} and surface marker phenotype of T cells at days 0, 4, and 7 following transfection, respectively. For each sample, 1×10^5 cells were harvested in duplicate or triplicate, centrifuged, and washed once in FACS buffer. The cells were then transferred to a v-bottom 96-well plate for staining with T_{SCM} or surface marker phenotype antibody master mix, prepared in FACS buffer, and incubated for 20 min at 4°C in the dark. For T_{SCM} analysis, cells were incubated in a master mix solution of FACS buffer containing anti-CD3, anti-CD4, anti-CD8, anti-CD45RA, anti-CD45RO, anti-CD62L, anti-CD95, and anti-CCR7. For surface marker characterization, cells were incubated

in a master mix solution of FACS buffer containing anti-CD3, anti-CD4, anti-CD8, anti-CTLA4, anti-LAG3, anti-PD-1, anti-TIGIT, and anti-TIM3. For analysis, live cells were gated using Zombie Aqua vital dye exclusion (BioLegend, 423101), and post-acquisition samples were analyzed using NovoExpress software (version 1.6.1). Flow cytometry analysis for T cells was performed on live single cells gated as CD3$^+$, CD4$^+$, or CD8$^+$, followed by the gating on each of the specific markers. T_{SCM} cells were classified as CD45RA$^+$, CD45RO$^-$, CD62L$^+$, CCR7$^+$, and CD95$^+$. Gates were determined by FMO controls for each specific marker. A comprehensive list of these antibody markers and others can be found in Table 2.

Apoptosis measurement

Apoptosis was assessed in transfected cells using a modified assay, incorporating Nucview 405 Caspase 3 Substrate (Biotium, 10407) and the Live/Dead Viability/Cytotoxicity Kit (Thermo Fisher, L3224). The dyes were allowed to come to room temperature and diluted to the desired concentration. Calcein AM, 4 mM, was first diluted 1:150 in DMSO and then further diluted 1:20 in PBS to achieve a final working stock of 1:3,000 (1.33 μM), and 2 mM ethidium homodimer was diluted 1:10 in PBS to create a 0.2-mM staining solution. Samples of 1×10^5 in 100 μL culture medium were collected 30 min post-transfection via Solupore or electroporation and subjected to apoptosis analysis. This involved the addition of 1 μL 1 mM Nucview 405 Caspase 3 Substrate, 3 μL 0.2 mM ethidium, and 1 μL 1.33 μM Calcein AM for 15 min in the dark at room temperature. Subsequently, the samples were analyzed by flow cytometer, detecting calcein (fluorescein isothiocyanate [FITC]), ethidium (PE-Texas Red), and NucView-405 (Pacific blue).

In vitro cytotoxicity assay

CAR-T cell cytotoxicity was assessed using the Incucyte S3 Live-Cell Analysis System (Sartorius). To evaluate the killing efficacy of effector CAR-T cells, Nalm-6 or Raji CD19$^+$ target cells were labeled with the Incucyte Green Cytotoxicity Reagent (Sartorius, 4633), which fluoresces upon cell death. Nalm-6 or Raji cells were cultured in RPMI with 10% FBS, maintained at $<0.9 \times 10^6$ cells/mL with passage <20. Prior to cytotoxicity assays, target cells were transferred to complete TexMACS media (without IL-2) containing 5% human AB serum and cultured overnight to prevent serum shock. On the assay day, Nalm-6 or Raji cells were centrifuged and resuspended at 4×10^5 cells/mL in TexMACS with green cytotoxicity reagent (250 nM). Cell suspension, 100 μL, was added to row 1 of a flat-bottom 96-well plate, while 50 μL TexMACS with green cytotoxicity reagent was added to the rows below. Serial dilutions were performed by transferring 50 μL suspension between rows. Cells were incubated for 10 min in the dark to incorporate the green dye. The target cells were then overlaid with 2×10^4 untransfected, Solupore-transfected, or electroporation-transfected CAR-T cells and control untransfected non-transduced cells. T cell-only and target cell-only wells were also included. The cell plate was placed in the Incucyte, and images were captured every 30 min for 24 or 48 h. Analysis was performed using Incucyte 2022B Rev2 software, and results were graphed as a ratio of cytotoxicity relative to baseline cytotoxicity at 0 h (Nalm-6) and 1 h (Raji cells).

Table 2. Flow cytometry antibodies

Marker	Conjugate	Host	Reactivity	Clone	Manufacturer	Catalog no.
KO efficiency						
CD3	phycoerythrin/cyanine7	mouse immunoglobulin G1, κ	human	SK7	BioLegend	344816
CD7	FITC	mouse immunoglobulin G2a, κ	human	CD7-6B7	BioLegend	343104
HLA-A, -B, -C	allophycocyanin	mouse immunoglobulin G2a, κ	human	W6/32	BioLegend	311410
T cell phenotyping						
CD3	Brilliant Violet 421	mouse immunoglobulin G2a, κ	human	OKT3	BioLegend	317344
CD4	phycoerythrin/cyanine7	mouse immunoglobulin G2b, κ	human	OKT4	BioLegend	317414
CD8	Super Bright 780	mouse immunoglobulin G2a, κ	human	OKT8	Invitrogen	78-0086-42
CD45RA	FITC	mouse immunoglobulin G2b, κ	human	HI100	BioLegend	983002
CD45RO	allophycocyanin REAfinity	human immunoglobulin G1	human	REA611	Miltenyi	130-113-556
CD62L (L-selectin)	Super Bright 600	mouse immunoglobulin G1, κ	human	DREG56	Invitrogen	63-0629-42
CD95 (FAS)	allophycocyanin /cyanine7	mouse immunoglobulin G1, κ	human	DX2	BioLegend	305636
CCR7 (CD197)	phycoerythrin/Dazzle 594	mouse immunoglobulin G2a, κ	human	G043H7	BioLegend	353236
CTLA-4	Brilliant Violet 605	mouse immunoglobulin G2a, κ	human	BNI3	BioLegend	369610
LAG-3 (CD223)	phycoerythrin/Dazzle 594	mouse immunoglobulin G1, κ	human	11C3C65	BioLegend	369332
PD-1 (CD279)	Alexa Fluor 488	mouse immunoglobulin G1, κ	human	EH12.2H7	BioLegend	329936
TIGIT (VSTM3)	allophycocyanin /cyanine7	mouse immunoglobulin G2a, κ	human	A15153G	BioLegend	372734
TIM-3 (CD366)	allophycocyanin	mouse immunoglobulin G1, κ	human	A18087E	BioLegend	364804
In vivo study						
CD3	Brilliant Violet 510	mouse immunoglobulin G1, κ	human	SK7	BioLegend	344828
CD4	BD Horizon BUV496	mouse immunoglobulin G1, κ	human	SK3 (Leu3a)	BD Biosciences	612936
CD7	phycoerythrin	mouse immunoglobulin G2a, κ	human	CD7-6B7	BioLegend	343106
CD8	BD Horizon BUV395	mouse immunoglobulin G1, κ	human	RPA-T8	BD Biosciences	563795
CD25	Brilliant Violet 711	mouse immunoglobulin G1, κ	human	M-A251	BioLegend	356138
CD45	BD Horizon BUV805	mouse immunoglobulin G1, κ	human	HI30	BD Biosciences	612891
CD45	Alexa Fluor 700	rat immunoglobulin G2b, κ	mouse	30-F11	BioLegend	103128
CD69	Brilliant Violet 421	mouse immunoglobulin G1, κ	human	FN50	BioLegend	310930
CD107a (LAMP-1)	allophycocyanin	mouse immunoglobulin G1, κ	human	H4A3	BioLegend	328620
PD-1 (CD279)	Brilliant Violet 785	mouse immunoglobulin G1, κ	human	EH12.2H7	BioLegend	329930
β2-Microglobulin	FITC	mouse immunoglobulin G1, κ	human	A17082A	BioLegend	395706

Cell binding avidity assays

The strength of cell-target binding of untransfected, Solupore-transfected, or electroporation-transfected CAR-T cells was measured using the z-movi Cell Avidity Analyzer (LUMICKS). Cellular avidity was measured across multiple donors 24 and 48 h post-transduction or on CAR-T cells 24 h post-thaw, cryopreserved at 24 h post-transduction, and stored at $-80°C$ until ready for analysis. CD19 expressing Raji tumor cells were seeded in a z-Movi poly-L-lysine-coated microfluidic chip for at least 2 h. Effector CAR-T cells were biologically normalized for transduction efficiency and added to the chip at 1×10^7 cells/mL and allowed to adhere with targets for an optimized interaction time of 5 min prior to initializing the acoustic force ramp. During the force ramp, the z-Movi device utilizes a bright-field microscope to capture a time series of images. Detachment data were acquired using z-Movi Tracking version 1.6.0, and post-experiment analysis was carried out with Ocean software. The avidity score was calculated by the software, represented as the ratio of mean relative force required to detach Solupore CAR-T cells from the Raji CD19+ tumor monolayer compared to untransfected, electroporation-transfected, or non-transduced controls. All experiments and analysis followed the manufacturers' recommendations.

Seahorse metabolic profiling

T cell metabolism was analyzed using Agilent Seahorse XF HS Analyzer and T Cell Metabolic Profiling Kit (Agilent, 103771-100), according to the manufacturer's instructions. On the day prior to the assay, a Seahorse XFp sensor cartridge (Agilent, 103721-100) was hydrated with tissue culture-grade water at 37°C in a non-CO_2 incubator overnight. An XFp poly-D-lysine (PDL)-coated miniplate (Agilent, 103721-100) and an aliquot of calibrant were also

incubated at $37°C$ in a non-CO_2 incubator overnight. On the day of the assay, the water was replaced with pre-warmed calibrant and incubated in a non-CO_2 incubator for a further 60 min. Seahorse RPMI assay medium was prepared according to the manufacturer's instructions; supplemented with glucose (10 mM), pyruvate (1 mM), and glutamine (2 mM); and warmed to $37°C$. Untransfected, Solupore-transfected, or electroporation-transfected CD3 T cells were counted, and 1×10^5 cells/well were plated in duplicate or triplicate in 200-µL assay medium onto the PDL miniplate inside a BSC. The PDL miniplate with cells was incubated in a $37°C$ non-CO_2 incubator for 45–60 min prior to the assay. Assay medium was used to reconstitute the metabolic inhibitor loading solutions supplied in the kit (103771-100). A total of 25 µL was loaded into ports A, B, and C of each well of the sensor cartridge for a final concentration of oligomycin A (13.5 µM), BAM15 (25 µM), and rotenone/antimycin A (5.5 µM). The assay was run on the Seahorse XF analyzer according to the designed T cell metabolic profiling template. Seahorse Analytics web-based software and GraphPad Prism were used for data analysis and graph generation.

Cytokine array

Solupore- or electroporation-transfected CD3^{+} T cells were either stimulated with PMA (Merck, P1585) and ionomycin (Merck, I9657) or transduced populations were co-cultured with Raji cells for cytokine analysis using the LEGENDPlex Human CD8/NK Panel Kit (BioLegend, 741187). Cell-free supernatants were harvested from 24-well G-Rex on day 4 post-transfection, following two rounds of PMA (10 ng/mL) and ionomycin (250 ng/mL) stimulation on days 0 and 3. For co-culture supernatants, CD3 T cells were transduced with anti-CD19 CAR Lentiviral vector (LVV) at an MOI of 3 at 2 days post-transfection and co-cultured at a 1:1 ratio with Raji cells for 24 h. The supernatants were harvested in duplicate or triplicate, centrifuged to remove cell debris, and stored at $-80°C$ until the day of analysis. The concentration of IL-2, IL-4, IL-10, IL-6, IL-17A, tumor necrosis factor-α, sFas, sFasL, IFN-γ, granzyme A, granzyme B, perforin, and granulysin in the supernatants were determined using the LEGENDplex kit according to the manufacturer's instructions. Supernatants were thawed at room temperature and diluted with assay buffer (1:2 for co-culture and up to 1:4 for PMA/ionomycin). In brief, on the day of assay, 25 µL diluted sample or standard, 25 µL assay buffer, and 25 µL mixed beads were added to the appropriate wells of a v-bottom 96-well plate and shaken at 700 rpm using a thermo-shaker (Grant-Bio PCMT HC18) for 2 h at room temperature and protected from light. The samples were then centrifuged and washed twice in wash buffer, and 25 µL detection antibodies were added to each well and shaken at 700 rpm using a thermo-shaker protected from light. After 1 h, 25 µL streptavidin-PE was added to each well and incubated for a further 30 min. The plate was then centrifuged, washed once in wash buffer, and resuspended in 150 µL wash buffer, and samples were analyzed by flow cytometry. Flow cytometry standard files were exported for analysis using the LEGENDplex data analysis software Qognit. Results were analyzed in Microsoft Excel and graphed using GraphPad Prism (version 9.0).

In vivo murine CAR-T cell-efficacy study

CAR-T cells were manufactured for an *in vivo* mouse study using either the Solupore system or electroporation as a transfection mechanism for CD3 (TRAC), B2M, and CD7 RNP based knock-out. After transfection and triple edit, cells were further edited to integrate and express the anti-CD19 CAR gene using lentiviral transduction. Four treatment groups of untransfected non-transduced, untransfected CAR, Solupore CAR, and electroporation CAR (79%–84% CAR[+]) were cryopreserved as described previously at $-150°C$ and shipped to The Jackson Laboratory (California) for the *in vivo* CAR-T cell-efficacy study. Female NOD.Cg-*Prkdcscid H2-K1b-tm1Bpe H2-Ab1g7-em1Mvw H2-D1b-tm1Bpe Il2rgtm1Wjl*/SzJ (JAX, 025216 [NSG DKO, major histocompatibility complex class I/II]) mice at approximately 8–10 weeks of age were used for this study. Raji cells were maintained in the log phase of growth, with cell density $<0.9 \times 10^6$ cells/mL in 5% CO_2 at $37°C$ until enough cells were cultured to engraft all study mice. Mice were weighed and distributed into treatment groups based on averaging body weight. On study day 0, 104 mice were engrafted intravenously at 0.25×10^6 cells per mouse through the tail vein with Raji-LUC cancer cells. On study day 3, cryopreserved CAR-T cells were thawed, and 12 groups of mice were dosed intravenously with the 4 CAR-T cell treatment groups at 3 concentrations (4×10^6, 2×10^6, and 1×10^6 cells per mouse). CAR-T cells were thawed in a $37°C$ water bath in batches by group and transferred to TexMACS media containing 5% human serum, centrifuged at 350 rcf for 7 min, and resuspended in TexMACS with 5% human serum with IL-2 for counting. Once counted, the cell density was adjusted to 1×10^6 cells/mL and rested in the incubator for 4 h at $37°C$ and 5% CO_2. After 4 h, cells were centrifuged at 350 rcf for 7 min and resuspended in $37°C$ PBS to achieve 2.67×10^7 cells/mL for injection. The ready-to-inject cells were placed on ice and transferred for injections. A total of 150 µL of 2.67×10^7 cells/mL were injected for a top CAR-T dose of 4×10^6 cells per mouse and further diluted 1:2 and 1:4 in PBS to achieve 2×10^6 and 1×10^6 cells per mouse groups, respectively. Mice were removed from the cage for body weight measurements twice per week and detailed clinical observations three times per week. Mice were imaged on study days 4, 7, 13, 18, 20, and 25 using the Xenogen IVIS-Lumina system. Retro-orbital blood (55 µL) was collected from all mice on study days 7, 13, and 18 into K2-EDTA tubes. The collected whole blood was processed for flow cytometer analysis. The primary endpoint was tumor burden reduction, the secondary endpoint was engraftment of CAR-T cells, and the tertiary endpoint was the %KO cells at the terminal endpoint of the study (day 26) in comparison to %KO cells dosed.

Flow cytometry for *ex vivo* whole-blood and tissue samples

For flow cytometry analysis, samples of whole blood (obtained by retro-orbital bleed on study days 7, 13, and 18 and cardiac bleed post-CO_2 asphyxiation on study day 26) were processed, acquired, and analyzed by The Jackson Laboratory. In brief, samples of 50 µL were incubated with a surface antibody mix of anti-CD3, anti-CD4, anti-CD8, anti-CD25, anti-CD45, anti-CD69, anti-CD107a, anti-PD-1, anti-CD7 anti-B2M, and anti-mouse-CD45 in Brilliant Stain Buffer (BD Biosciences, 563794) for 30 min in the dark at $4°C$. After

the staining, samples were lysed with 500 μL 1× Pharm Lyse ammonium chloride solution (BD Biosciences, 555899) for 15 min in the dark at room temperature. Samples were then washed twice in Dulbecco's PBS without Ca^{2+} and Mg^{2+} (DPBS-CMF). Centrifugation after each wash was at 400 rcf for 5 min with brake. Cells were then resuspended in 150 μL 1× DPBS-CMF with 7-AAD dye (BD Biosciences, 559925) and 25 μL Countbright beads (Invitrogen, C36950) were added before acquiring on FACSSymphony A5 SE flow cytometer (BD Biosciences). For analysis, live cells were gated using 7-AAD vital dye exclusion, and post-acquisition, samples were analyzed using BD FACSDiva software (version 9.6). Flow cytometry analysis for cells was performed as live cells gated on $CD45^+$, $CD3^+$, or $CD3^-$, then $CD4^+$ or $CD8^+$, followed by gating each specific marker. CAR-T cell engraftment was defined by percentage of human $CD45^+$ T cells; of these, the activated T cells were characterized by $CD25^+$, $CD69^+$ expression, and exhausted or cytotoxic T cells were identified based on their expression of markers PD-1 and CD107a. TKO efficiency was evaluated by identifying $CD3^-$, $CD7^-$, and $B2M^-$ populations. Gates were determined by three fluorescence minus multiple (FMM) controls, FMM1 (CD69/PD-1), FMM2 (CD25/CD107a), and FMM3 (CD7/B2M).

At the terminal endpoint, on study day 26, the remaining surviving animals were euthanized by CO_2 asphyxiation. In line with the BD Biosciences "Preparation of Murine Splenocytes" procedure, the spleen was excised and processed into a single cell suspension in MACS cell storage solution (Miltenyi, 130-130-263) and stored in $4°C$ for analysis by flow cytometry. In short, the cell suspension was prepared by pressing the spleen through a strainer, washing with PBS, and centrifuging at 1,600 rpm for 5 min. The supernatant was removed, and the cell pellet was resuspended in lysing solution for 2 min at $37°C$. This was followed by washing in 30 mL PBS and resuspending the pellet in PBS to a density of 2×10^6 cells/mL. Samples were incubated in the surface antibody mix, and samples were acquired and analyzed as described above.

In vivo image acquisition and analysis
Tumor progression of Raji-LUC was monitored by bioluminescence imaging (BLI) using a Xenogen Lumina IVIS (PerkinElmer). For BLI IVIS, mice with Raji-LUC engraftment were anesthetized with XGI-8 gas, injected intraperitoneally with 150 mg/kg XenoLight D-Luciferin – K^+ Salt Bioluminescent Substrate (PerkinElmer, 122796) and placed into the IVIS imaging chamber. Mice were imaged in sequence from the ventral position on study days 4, 7, 13, 18, 20, and 25. For BLI quantification, the whole-body region of interest (ROI) was selected, and BLI was recorded as radiance (photons/s/cm²/sr). Total radiance was calculated for all groups and time points, and the brightness and scale of the images were adjusted in Living Image version 4.8.0 software.

Statistical analysis
Values are given as mean ± SD of at least three donors unless otherwise noted. All analyses were performed using GraphPad Prism version 10.0 for Windows (GraphPad Software, www.graphpad. com). Statistical significance between Solupore and electroporation experimental groups was determined using paired and unpaired t tests for parametric data and Wilcoxon matched-pairs signed rank or Mann-Whitney U test for non-parametric data. Comparisons of multiple groups were performed using a one- or two-way ANOVA. $p < 0.05$ was considered significant and is designated with an asterisk in all figures: ns $p > 0.05$; *$p \leq 0.05$; **$p \leq 0.01$; ***$p \leq 0.001$; ****$p \leq 0.0001$.

AUTHOR CONTRIBUTIONS
A.O., S.C., and A.M. conducted the analytical experiments. J.F. designed the experiments, and J.F. and S.C. wrote the manuscript, reviewed by L.O. J.F., A.O., and L.O. carried out the data analysis and interpretation. E.H. and D.M. conducted the sample preparation for analysis. G.P.J. and K.M. were responsible for the cell culture work. L.G., T.K., and K.S. conducted the transfection process experiments, supported by A.O., E.H., and D.M. M.W.L. supported the cell avidity measurements on the cryopreserved samples at the University College London (UCL) Royal Free Hospital, London. Murine experiments were performed at The Jackson Laboratory, Sacramento.

REFERENCES
1. Davila, M.L., Riviere, I., Wang, X., Bartido, S., Park, J., Curran, K., Chung, S.S., Stefanski, J., Borquez-Ojeda, O., Olszewska, M., et al. (2014). Efficacy and toxicity management of 19-28z CAR T cell therapy in B cell acute lymphoblastic leukemia. Sci. Transl. Med. 6, 224ra25.

2. Maude, S.L., Frey, N., Shaw, P.A., Aplenc, R., Barrett, D.M., Bunin, N.J., Chew, A., Gonzalez, V.E., Zheng, Z., Lacey, S.F., et al. (2014). Chimeric antigen receptor T cells for sustained remissions in leukemia. N. Engl. J. Med. 371, 1507–1517.

3. Lee, D.W., Kochenderfer, J.N., Stetler-Stevenson, M., Cui, Y.K., Delbrook, C., Feldman, S.A., Fry, T.J., Orentas, R., Sabatino, M., Shah, N.N., et al. (2015). T cells expressing CD19 chimeric antigen receptors for acute lymphoblastic leukaemia in children and young adults: a phase 1 dose-escalation trial. Lancet 385, 517–528.

4. Turtle, C.J., Hanafi, L.A., Berger, C., Gooley, T.A., Cherian, S., Hudecek, M., Sommermeyer, D., Melville, K., Pender, B., Budiarto, T.M., et al. (2016). CD19 CAR-T cells of defined CD4+:CD8+ composition in adult B cell ALL patients. J. Clin. Invest. 126, 2123–2138.

5. Maude, S.L., Laetsch, T.W., Buechner, J., Rives, S., Boyer, M., Bittencourt, H., Bader, P., Verneris, M.R., Stefanski, H.E., Myers, G.D., et al. (2018). Tisagenlecleucel in

Children and Young Adults with B-Cell Lymphoblastic Leukemia. N. Engl. J. Med. *378*, 439–448.

6. Park, J.H., Rivière, I., Gonen, M., Wang, X., Sénéchal, B., Curran, K.J., Sauter, C., Wang, Y., Santomasso, B., Mead, E., et al. (2018). Long-Term Follow-up of CD19 CAR Therapy in Acute Lymphoblastic Leukemia. N. Engl. J. Med. *378*, 449–459.

7. Garcia, J., Daniels, J., Lee, Y., Zhu, I., Cheng, K., Liu, Q., Goodman, D., Burnett, C., Law, C., Thienpont, C., et al. (2024). Naturally occurring T cell mutations enhance engineered T cell therapies. Nature *626*, 626–634.

8. Negishi, S., Girsch, J.H., Siegler, E.L., Bezerra, E.D., Miyao, K., and Sakemura, R.L. (2023). Treatment strategies for relapse after CAR T-cell therapy in B cell lymphoma. Front. Pediatr. *11*, 1305657.

9. Li, Y., Ming, Y., Fu, R., Li, C., Wu, Y., Jiang, T., Li, Z., Ni, R., Li, L., Su, H., and Liu, Y. (2022). The pathogenesis, diagnosis, prevention, and treatment of CAR-T cell therapy-related adverse reactions. Front. Pharmacol. *13*, 950923.

10. Sterner, R.C., and Sterner, R.M. (2021). CAR-T cell therapy: current limitations and potential strategies. Blood Cancer J. *11*, 69.

11. Gattinoni, L., Zhong, X.S., Palmer, D.C., Ji, Y., Hinrichs, C.S., Yu, Z., Wrzesinski, C., Boni, A., Cassard, L., Garvin, L.M., et al. (2009). Wnt signaling arrests effector T cell differentiation and generates CD8+ memory stem cells. Nat. Med. *15*, 808–813.

12. Gattinoni, L., Lugli, E., Ji, Y., Pos, Z., Paulos, C.M., Quigley, M.F., Almeida, J.R., Gostick, E., Yu, Z., Carpenito, C., et al. (2011). A human memory T cell subset with stem cell-like properties. Nat. Med. *17*, 1290–1297.

13. Gattinoni, L., Klebanoff, C.A., Palmer, D.C., Wrzesinski, C., Kerstann, K., Yu, Z., Finkelstein, S.E., Theoret, M.R., Rosenberg, S.A., and Restifo, N.P. (2005). Acquisition of full effector function in vitro paradoxically impairs the in vivo antitumor efficacy of adoptively transferred CD8+ T cells. J. Clin. Invest. *115*, 1616–1626.

14. Klebanoff, C.A., Gattinoni, L., Torabi-Parizi, P., Kerstann, K., Cardones, A.R., Finkelstein, S.E., Palmer, D.C., Antony, P.A., Hwang, S.T., Rosenberg, S.A., et al. (2005). Central memory self/tumor-reactive CD8+ T cells confer superior antitumor immunity compared with effector memory T cells. Proc. Natl. Acad. Sci. USA *102*, 9571–9576.

15. Hinrichs, C.S., Borman, Z.A., Cassard, L., Gattinoni, L., Spolski, R., Yu, Z., Sanchez-Perez, L., Muranski, P., Kern, S.J., Logun, C., et al. (2009). Adoptively transferred effector cells derived from naive rather than central memory CD8+ T cells mediate superior antitumor immunity. Proc. Natl. Acad. Sci. USA *106*, 17469–17474.

16. Wang, X., Wong, C.W., Urak, R., Taus, E., Aguilar, B., Chang, W.C., Mardiros, A., Budde, L.E., Brown, C.E., Berger, C., et al. (2016). Comparison of naïve and central memory derived CD8(+) effector cell engraftment fitness and function following adoptive transfer. OncoImmunology *5*, e1072671.

17. Gattinoni, L., Speiser, D.E., Lichterfeld, M., and Bonini, C. (2017). T memory stem cells in health and disease. Nat. Med. *23*, 18–27.

18. Klebanoff, C.A., Gattinoni, L., Palmer, D.C., Muranski, P., Ji, Y., Hinrichs, C.S., Borman, Z.A., Kerkar, S.P., Scott, C.D., Finkelstein, S.E., et al. (2011). Determinants of successful CD8+ T-cell adoptive immunotherapy for large established tumors in mice. Clin. Cancer Res. *17*, 5343–5352.

19. Sabatino, M., Hu, J., Sommariva, M., Gautam, S., Fellowes, V., Hocker, J.D., Dougherty, S., Qin, H., Klebanoff, C.A., Fry, T.J., et al. (2016). Generation of clinical-grade CD19-specific CAR-modified CD8+ memory stem cells for the treatment of human B-cell malignancies. Blood *128*, 519–528.

20. Ikegawa, S., Sperling, A.S., Ansuinelli, M., Nikiforow, S., Quinn, D., Bu, D., Mataraza, J., Pearson, D., Rispoli, L., Credi, M.A., et al. (2023). T-Charge™ Manufacturing of the Anti-BCMA CAR-T, Durcabtagene Autoleucel (PHE885), Promotes Expansion and Persistence of CAR-T Cells with High TCR Repertoire Diversity. Blood *142*, 3469.

21. Du, J., Qiang, W., Lu, J., Jia, Y., He, H., Liu, J., Guo, P., Yang, Y., Feng, Z., Jin, L., et al. (2023). Updated Results of a Phase I Open-Label Single-Arm Study of Dual Targeting BCMA and CD19 Fastcar-T Cells (GC012F) As First-Line Therapy for Transplant-Eligible Newly Diagnosed High-Risk Multiple Myeloma. Blood *142*, 1022.

22. Du, J., Fu, W.-J., Jiang, H., Dong, B., Gao, L., Liu, L., Ge, J., He, A., Li, L., Lu, J., et al. (2023). Updated results of a phase I, open-label study of BCMA/CD19 dual-targeting fast CAR-T GC012F for patients with relapsed/refractory multiple myeloma (RRMM). J. Clin. Oncol. *41*, 8005.

23. Mehta, P.H., Fiorenza, S., Koldej, R.M., Jaworowski, A., Ritchie, D.S., and Quinn, K.M. (2021). T Cell Fitness and Autologous CAR T Cell Therapy in Haematologic Malignancy. Front. Immunol. *12*, 780442.

24. Neumann, E., Schaefer-Ridder, M., Wang, Y., and Hofschneider, P.H. (1982). Gene transfer into mouse lyoma cells by electroporation in high electric fields. Embo J. *1*, 841–845.

25. Tsong, T.Y. (1991). Electroporation of cell membranes. Biophys. J. *60*, 297–306.

26. Gehl, J. (2003). Electroporation: theory and methods, perspectives for drug delivery, gene therapy and research. Acta Physiol. Scand. *177*, 437–447.

27. Venslauskas, M.S., and Šatkauskas, S. (2015). Mechanisms of transfer of bioactive molecules through the cell membrane by electroporation. Eur. Biophys. J. *44*, 277–289.

28. Batista Napotnik, T., Polajžer, T., and Miklavčič, D. (2021). Cell death due to electroporation - A review. Bioelectrochemistry *141*, 107871.

29. Kavanagh, H., Dunne, S., Martin, D.S., McFadden, E., Gallagher, L., Schwaber, J., Leonard, S., and O'Dea, S. (2021). A novel non-viral delivery method that enables efficient engineering of primary human T cells for ex vivo cell therapy applications. Cytotherapy *23*, 852–860.

30. O'Dea, S., Annibaldi, V., Gallagher, L., Mulholland, J., Molloy, E.L., Breen, C.J., Gilbert, J.L., Martin, D.S., Maguire, M., and Curry, F.R. (2017). Vector-free intracellular delivery by reversible permeabilization. PLoS One *12*, e0174779.

31. Rangel Rivera, G.O., Knochelmann, H.M., Dwyer, C.J., Smith, A.S., Wyatt, M.M., Rivera-Reyes, A.M., Thaxton, J.E., and Paulos, C.M. (2021). Fundamentals of T Cell Metabolism and Strategies to Enhance Cancer Immunotherapy. Front. Immunol. *12*, 645242.

32. Yang, K., Neale, G., Green, D.R., He, W., and Chi, H. (2011). The tumor suppressor Tsc1 enforces quiescence of naive T cells to promote immune homeostasis and function. Nat. Immunol. *12*, 888–897.

33. Chang, C.H., Curtis, J.D., Maggi, L.B., Jr., Faubert, B., Villarino, A.V., O'Sullivan, D., Huang, S.C.C., van der Windt, G.J.W., Blagih, J., Qiu, J., et al. (2013). Posttranscriptional control of T cell effector function by aerobic glycolysis. Cell *153*, 1239–1251.

34. Geltink, R.I.K., Kyle, R.L., and Pearce, E.L. (2018). Unraveling the Complex Interplay Between T Cell Metabolism and Function. Annu. Rev. Immunol. *36*, 461–488.

35. Cunningham, C.A., Bergsbaken, T., and Fink, P.J. (2017). Cutting Edge: Defective Aerobic Glycolysis Defines the Distinct Effector Function in Antigen-Activated CD8(+) Recent Thymic Emigrants. J. Immunol. *198*, 4575–4580.

36. Larson, R.C., Kann, M.C., Bailey, S.R., Haradhvala, N.J., Llopis, P.M., Bouffard, A.A., Scarfó, I., Leick, M.B., Grauwet, K., Berger, T.R., et al. (2022). CAR T cell killing requires the IFNγR pathway in solid but not liquid tumours. Nature *604*, 563–570.

37. Chockley, P.J., Ibanez-Vega, J., Krenciute, G., Talbot, L.J., and Gottschalk, S. (2023). Synapse-tuned CARs enhance immune cell anti-tumor activity. Nat. Biotechnol. *41*, 1434–1445.

38. Lee, L., Lim, W.C., Galas-Filipowicz, D., Fung, K., Taylor, J., Patel, D., Akbar, Z., Alvarez Mediavilla, E., Wawrzyniecka, P., Shome, D., et al. (2023). Limited efficacy of APRIL CAR in patients with multiple myeloma indicate challenges in the use of natural ligands for CAR T-cell therapy. J. Immunother. Cancer *11*, e006699.

39. Zhang, Y., Patel, R.P., Kim, K.H., Cho, H., Jo, J.C., Jeong, S.H., Oh, S.Y., Choi, Y.S., Kim, S.H., Lee, J.H., et al. (2023). Safety and efficacy of a novel anti-CD19 chimeric antigen receptor T cell product targeting a membrane-proximal domain of CD19 with fast on- and off-rates against non-Hodgkin lymphoma: a first-in-human study. Mol. Cancer *22*, 200.

40. Wang, Y., Buck, A., Piel, B., Zerefa, L., Murugan, N., Coherd, C.D., Miklosi, A.G., Johal, H., Bastos, R.N., Huang, K., et al. (2024). Affinity fine-tuning anti-CAIX CAR-T cells mitigate on-target off-tumor side effects. Mol. Cancer *23*, 56.

41. Todorovic, Z., Todorovic, D., Markovic, V., Ladjevac, N., Zdravkovic, N., Djurdjevic, P., Arsenijevic, N., Milovanovic, M., Arsenijevic, A., and Milovanovic, J. (2022). CAR T Cell Therapy for Chronic Lymphocytic Leukemia: Successes and Shortcomings. Curr. Oncol. *29*, 3647–3657.

42. Waldman, A.D., Fritz, J.M., and Lenardo, M.J. (2020). A guide to cancer immunotherapy: from T cell basic science to clinical practice. Nat. Rev. Immunol. *20*, 651–668.

43. Harris, E., and Elmer, J.J. (2021). Optimization of electroporation and other non-viral gene delivery strategies for T cells. Biotechnol. Prog. *37*, e3066.

44. Ferrari, D., Wesselborg, S., Bauer, M.K., and Schulze-Osthoff, K. (1997). Extracellular ATP activates transcription factor NF-kappaB through the P2Z purinoreceptor by selectively targeting NF-kappaB p65. J. Cell Biol. *139*, 1635–1643.

45. Gozuacik, D., Bialik, S., Raveh, T., Mitou, G., Shohat, G., Sabanay, H., Mizushima, N., Yoshimori, T., and Kimchi, A. (2008). DAP-kinase is a mediator of endoplasmic reticulum stress-induced caspase activation and autophagic cell death. Cell Death Differ. *15*, 1875–1886.

46. Krysko, D.V., Vanden Berghe, T., D'Herde, K., and Vandenabeele, P. (2008). Apoptosis and necrosis: detection, discrimination and phagocytosis. Methods *44*, 205–221.

47. Krysko, D.V., and Vandenabeele, P. (2010). Clearance of dead cells: mechanisms, immune responses and implication in the development of diseases. Apoptosis *15*, 995–997.

48. St Paul, M., and Ohashi, P.S. (2020). The Roles of CD8(+) T Cell Subsets in Antitumor Immunity. Trends Cell Biol. *30*, 695–704.

49. van Stipdonk, M.J., Lemmens, E.E., and Schoenberger, S.P. (2001). Naïve CTLs require a single brief period of antigenic stimulation for clonal expansion and differentiation. Nat. Immunol. *2*, 423–429.

50. Krawczyk, C.M., Holowka, T., Sun, J., Blagih, J., Amiel, E., DeBerardinis, R.J., Cross, J.R., Jung, E., Thompson, C.B., Jones, R.G., and Pearce, E.J. (2010). Toll-like receptor-induced changes in glycolytic metabolism regulate dendritic cell activation. Blood *115*, 4742–4749.

51. Masters, S.L., Dunne, A., Subramanian, S.L., Hull, R.L., Tannahill, G.M., Sharp, F.A., Becker, C., Franchi, L., Yoshihara, E., Chen, Z., et al. (2010). Activation of the NLRP3 inflammasome by islet amyloid polypeptide provides a mechanism for enhanced IL-1β in type 2 diabetes. Nat. Immunol. *11*, 897–904.

52. Zhou, R., Tardivel, A., Thorens, B., Choi, I., and Tschopp, J. (2010). Thioredoxin-interacting protein links oxidative stress to inflammasome activation. Nat. Immunol. *11*, 136–140.

53. O'Neill, L.A.J., Kishton, R.J., and Rathmell, J. (2016). A guide to immunometabolism for immunologists. Nat. Rev. Immunol. *16*, 553–565.

54. Li, W., Pan, X., Chen, L., Cui, H., Mo, S., Pan, Y., Shen, Y., Shi, M., Wu, J., Luo, F., et al. (2023). Cell metabolism-based optimization strategy of CAR-T cell function in cancer therapy. Front. Immunol. *14*, 1186383.

55. McKinney, E.F., and Smith, K.G.C. (2018). Metabolic exhaustion in infection, cancer and autoimmunity. Nat. Immunol. *19*, 213–221.

56. Bengsch, B., Johnson, A.L., Kurachi, M., Odorizzi, P.M., Pauken, K.E., Attanasio, J., Stelekati, E., McLane, L.M., Paley, M.A., Delgoffe, G.M., and Wherry, E.J. (2016). Bioenergetic Insufficiencies Due to Metabolic Alterations Regulated by the Inhibitory Receptor PD-1 Are an Early Driver of CD8(+) T Cell Exhaustion. Immunity *45*, 358–373.

57. Hukelmann, J.L., Anderson, K.E., Sinclair, L.V., Grzes, K.M., Murillo, A.B., Hawkins, P.T., Stephens, L.R., Lamond, A.I., and Cantrell, D.A. (2016). The cytotoxic T cell proteome and its shaping by the kinase mTOR. Nat. Immunol. *17*, 104–112.

58. Tan, H., Yang, K., Li, Y., Shaw, T.I., Wang, Y., Blanco, D.B., Wang, X., Cho, J.H., Wang, H., Rankin, S., et al. (2017). Integrative Proteomics and Phosphoproteomics Profiling Reveals Dynamic Signaling Networks and Bioenergetics Pathways Underlying T Cell Activation. Immunity *46*, 488–503.

59. Maalej, K.M., Merhi, M., Inchakalody, V.P., Mestiri, S., Alam, M., Maccalli, C., Cherif, H., Uddin, S., Steinhoff, M., Marincola, F.M., and Dermime, S. (2023). CAR-cell therapy in the era of solid tumor treatment: current challenges and emerging therapeutic advances. Mol. Cancer *22*, 20.